Journal of Hazardous Materials 409 (2021) 124987

Contents lists available at ScienceDirect

Journal of Hazardous Materials

journal homepage: www.elsevier.com/locate/jhazmat

Graphitic bio-char and bio-oil synthesis *via* hydrothermal carbonization-co-liquefaction of microalgae biomass (oiled/de-oiled) and multiple heavy metals remediations

Krishna Kumar Jaiswal [a], Vinod Kumar [a,*], Ravikant Verma [b], Monu Verma [c], Arvind Kumar [b], Mikhail S. Vlaskin [d,*], Manisha Nanda [e], Hyunook Kim [c]

[a] Algae Research & Bio-Energy Laboratory, Department of Chemistry, Uttaranchal University, Dehradun, Uttarakhand 248007, India
[b] Department of Ecology and Environmental Sciences, Pondicherry University, Puducherry 605014, India
[c] Department of Environmental Engineering, University of Seoul, Seoul 130743, South Korea
[d] Joint Institute for High Temperatures of the Russian Academy of Sciences, 13/2 Izhorskaya St, Moscow 125412, Russia
[e] Department of Biotechnology, Dolphin (P.G.) Institute of Biomedical and Natural Sciences, Dehradun 248001, India

ARTICLE INFO

Keywords:
Microalgae oiled and de-oiled biomass
HRAP
Hydrothermal carbonization-co-liquefaction (HTCL)
Bio-char and bio-oil
Multiple heavy metals remediation

ABSTRACT

Thermochemical transformation of microalgae biomass into graphitic bio-chars entices as proficient bio-adsorbents for heavy metal contaminants. This study explores the synergistic impact of *Chlorella sorokiniana* on biomass generation and wastewater remediation in high rate algae pond (HRAP). Biomass produced was applied for hydrothermal carbonization-co-liquefaction (HTCL). The structural and morphological characteristics of HTCL products (i.e. bio-chars and bio-oils) have been systematically studied by XRD, Raman, FTIR, elemental analyzer, SEM, BET, and ^{1}H NMR spectroscopy. The crystallite size of the graphite 2H indexing planes was to be 4.65 nm and 14.07 nm in the bio-chars of oiled biomass (MB-OB) and de-oiled biomass (MB-DOB), respectively. The increase in the I_D/I_G ratio of MB-DOB indicated the highly disordered graphitic structure due to the appearance of carbonyl, hydroxyl, and epoxy functionalities in the line of high C/N and low C/H ratio. Also, the multiple heavy metals remediation of MB-DOB revealed better efficiency as ~100% in 720 min. The kinetics analysis shows the correlation coefficient of pseudo-second-order is well fitted compared to the pseudo-first-order. The Langmuir adsorption model signifies the adsorption of heavy metal ions in a monolayer adsorption manner. The study proposes the microalgae bio-char potential for multiple heavy metals remediation alongside bio-oils.

1. Introduction

Microalgae are photosynthetic organisms similar to single-celled plants with habitats for various aquatic environments (Malavasi et al., 2020). They deal with the conversion of environmental CO_2 into O_2 in the presence of sunlight or artificial light and generate a large amount of biochemical components enriched with cellular energy (Jaiswal et al., 2020). Microalgae offer essential ecosystem and biomass services for diverse eco-friendly applications. They possess a rapid growth rate with notable biomass production and ensure the ability to grow in various types of wastewaters without competing with traditional agro-activities (Salama et al., 2017). In addition, the alarming threat to the existing ecosystem is due to industrialization and urbanization, as it discharges toxic heavy metals, wastes containing nitrogen, phosphorous, and others, as well as the release of CO_2 severely (Chowdhury et al., 2016). In this case, the concept of microalgae cultivation using many types of wastewaters (municipal, industrial, dairy, etc.) has been deliberated as a suitable scientific solution for renewable and sustainable developments (Jaiswal and Prasath, 2016; Cai et al., 2019; Sutherland and Ralph, 2019).

Recently, microalgae have received a lot of attention to the profitable cultivation of microalgae and energy-efficient biomass conversion technologies for biofuels for a variety of reasons (Choudhary et al., 2020). Despite enormous literature, experts endure the innovative and integrative design to develop cost-effective, biomass production processes, remediation of toxic metal contamination, wastewater

* Corresponding authors.
E-mail addresses: vinodkdhatwalia@gmail.com (V. Kumar), vlaskin@inbox.ru (M.S. Vlaskin).

https://doi.org/10.1016/j.jhazmat.2020.124987
Received 21 October 2020; Received in revised form 14 December 2020; Accepted 26 December 2020
Available online 29 December 2020

treatment, and biofuel production via energy-efficient thermochemical conversions (Fan et al., 2020; Lee et al., 2020). The favorable aspects of microalgae are multi-functionality, biological conversion competency, flexibility with the growth system, assimilation of nutrients from wastewater, CO_2 sequestration, and a large amount of biochemical constituents (Umamaheswari and Shanthakumar, 2016). To take this into account, cellular components (carbohydrates-lipids-proteins) are the driving factors in the generation of carbon-neutral biofuels such as bio-oil, biodiesel, bioethanol, biomethane, bio-hydrogen, and others (Jaiswal and Pandey, 2014; Jaiswal et al., 2020; Kumar et al., 2020).

Thermochemical technologies adopt thermal decomposition and chemical reform of organic cellular components in biofuels by carbonization, pyrolysis, hydrothermal liquefaction, gasification, and direct combustion (Kumar et al., 2017; Mathimani et al., 2019). The preparation of chars using biomass under the effect of temperature in water under pressure has been described as hydrothermal carbonization. In higher plants, the chemical properties are derived mainly from the components of lignin, cellulose, and hemicellulose. While microalgae biomass is not lignocellulose and differs in chemical properties in contrast to higher plants. The chemical properties of hydrothermal carbonization of microalgae biomass derived from the involvement of proteins, lipids and carbohydrates. Hydrothermal carbonization of microalgae biomass is a process to isolate products of 3 types, i.e., oils, chars, and nutrient-rich aqueous phase. The oils (fatty acids) obtained from the hydrothermal carbonization of microalgae biomass represent an enormous potential in the generation of liquid biofuels. The technologies mentioned above are very effective in the thermochemical conversion of microalgae biomass and generally take several seconds or minutes to generate a range of solid, liquid, or gaseous biofuels. However, hydrothermal carbonization-co-liquefaction technologies can be explored further in the field of microalgae biofuels. The biomass residues after microalgae lipid extraction are rich in carbohydrates, proteins, and a fraction of unused lipids. In general, lipid extraction is followed by two processes, i.e., from ruptured cells and intact cells. The recovery of intracellular lipids from cells of ruptured microalgae is highly efficient than that of intact cells. Biphasic solvent extraction selectively and immediately recovers non-polar triglycerides. Cell disruption for the extraction of intracellular lipids is a critical and efficient technique. Microalgae de-oiled biomass can be employed to generate bio-char solids, bio-oil liquids, and synthetic bio-gases as a renewable fuel, depending on the conversion process and temperatures (Liu et al., 2020).

However, substantial efforts have been cited on thermochemical conversion of numerous feedstocks such as lignocellulosic biomass, forestry waste, woods, pinewood, perennial grass, wheat straw, rice straw, rapeseed cake, apricot stone, coconut shell, hazelnut shell, chestnut shell, tea waste, coffee residue, fruit peel, etc. to produce bio-char (Wang et al., 2020). Even so, the concept of microalgae as an energy crop appeared to the spotlight for the manufacturing of carbon-rich solid biofuels i.e. microalgae bio-char via thermochemical processes. Bio-char is a pyrogenic solid fuel rich in carbon with high energy-density derived from the oxygen-limited thermal decomposition of biomasses in a closed system at a temperature range of 300–700 °C. It has a heterogeneous bio-char structure containing profused inorganic species which can be catalytically active by the thermal conversion technique. The solid black bio-char products are rich in carbon and have a pollution-free perspective in terms of environmental safety (Qin et al., 2020).

Furthermore, the inherent properties of bio-char include well-defined micro/meso/macro-porous structure, relatively high surface area, hydrophilic characteristics, surface binding oxygen functionalities (e.g. carboxyl, hydroxyl, carbonyl, and phenolic hydroxyl), efficient cation exchanger, and mineral constituents (e.g. Ca, K, Mg, and P) which expedite bio-char as an effective adsorbent in the remediation of organic or inorganic contaminants from the different wastewaters (Hu et al., 2019; Ma et al., 2017; Zhang et al., 2020). It has been observed that the application of microalgae bio-char could be a significant alternative to the nano-carbon such as carbon nanotubes, graphene, activated carbon, etc. to serve as highly efficient adsorbents for heavy metals (Jaiswal et al., 2018; Huang et al., 2019). Pb, Cu, Cd, and Ni are among the main toxic and carcinogenic heavy metals that could cause severe ecological and health complications, which incident from the discharge of mining, metallurgies, batteries, textiles, and paper industries (Carolin et al., 2017). Traditional wastewater treatment processes e.g. precipitation, ion exchange, electrocoagulation, membrane filtration, and packed-bed filtration have been established to be effective in removing heavy metal concentrations, but are allied with a higher operational budget and energy (Kehrein et al., 2020). Biological carbon-based adsorbents, such as bio-char, have been attracted as an excellent competitor to meet the necessity for remediation of toxic metals from different wastewater (Xiang et al., 2020).

Algal bio-char endows remarkable adsorption capacity to remove ammonical-N and various organic/inorganic contaminants from wastewater. Sorption of phosphates, nitrogen, and phosphorus has been also reported (Xiang et al., 2020). The bio-char enriched with essential macro-nutrients during wastewater remediation could be incorporated into the soil as an additive fertilizer. The algal bio-char has been studied to eliminate certain heavy metals such as Cu, Cd, and Zn ions from aqueous solutions (Ding et al., 2016). The bio-char prepared from freshwater macroalgae *Oedogonium* spp. has been used to remove metal ions from industrial effluents from the coal-fired power plant (Kidgell et al., 2014). Bio-char prepared from biomass of *Gracilaria* spp. treated with Fe has shown a strong affinity for oxyanions, e.g. As, Mo, and Se, which are difficult to eliminate using conventional practices (Johansson et al., 2016). The use of bio-char is becoming a low-cost, highly effective bio-sorbent for removing heavy metal contaminants (Cairns et al., 2020). This study investigated the generation of a novel crystalline structure of graphitic bio-chars (graphite 2H) with flakes and micro-rods morphology via the hydrothermal carbonization-co-liquefaction process of microalgae oiled/de-oiled biomass. The synergistic implication of the High Rate Algal Pond system with the integration of municipal wastewater has also been performed to produce microalgae *Chlorella sorokiniana* UUIND6 biomass together with wastewater treatment at the mini-pilot scale renewably and sustainably. The graphitic bio-chars were employed in the multiple-heavy-metal system for the remediation. The investigation on bio-oils revealed the higher aliphatic components of molecules dominant in bio-oils that contain more energy. Microalgae biomass generation using low-cost HRAP integrated with wastewater treatment offers an efficient, sustainable, and economical approach for biofuel production (Arora et al., 2020). This study aims to exploit the HRAP for the treatment of municipal wastewater without any dilution or pre-sterilization integrated with the subsequent utilization of microalgae biomass to produce graphitic bio-chars and bio-oils production. Graphitic bio-chars were applied to study the efficiency of multiple heavy metals remediation.

2. Experimental

2.1. Chemicals

The chemicals and reagents used to prepare standard media (BBM) for microalgae culture and biochemical analysis were purchased from HiMedia Laboratories Pvt. Ltd., India. Potassium bromide (FT-IR grade, ≥99% trace metals basis) and chloroform-d (99.8 atom % D) were obtained from Sigma-Aldrich Merck, India. Chloroform (ACS grade), dichloromethane (ACS grade), methanol (ACS grade), and sodium carbonate (ISO grade), copper(II) sulfate pentahydrate (ISO grade), nickel (II) nitrate hexahydrate (ACS grade), cobalt(II) nitrate hexahydrate (ISO grade) and cadmium chloride hemi(pentahydrate) (ISO grade) were

Fig. 1. Schematic representation of microalgae culture, hydrothermal carbonization-co-liquefaction and multiple heavy metals remediation.

procured from Merck Life Science Pvt. Ltd., India, and Milli-Q water was used for the experiment.

2.2. Microalgae and culture conditions with municipal wastewater

Freshwater green microalgae, *Chlorella sorokiniana* UUIND6 (GenBank accession number: KY780616) was previously isolated by our research group from the wastewater source at the Algae and Bioenergy Research Laboratory, Department of Chemistry, Uttaranchal University, Dehradun, Uttarakhand, India was maintained in Bold's Basal Media (BBM) at 25 ± 2 °C under white light LED illumination.

Municipal wastewater (MWW) was collected from the sewage channel of Prem Nagar, Dehradun, Uttarakhand (30°19′59″N 77°57′39″E) and allowed to settle down for 3–4 h to eliminate large solids/sediments. The physicochemical characterization of collected wastewater was performed by The Standard Methods for the Examination of Water and Wastewater (APHA, 2012). The experimental setup was designed to produce low-cost microalgae biomass integrated with municipal wastewater remediation in a 100 L volume capacity of artificial high rate algae pond (HRAP) (100 L × 50 W × 20H). An indoor HRAP culture system for microalgae was established in an artificial pond with white light LED illumination (300 μmol m^{-2} s^{-1}) and a photoperiod (18 h light and 6 h dark) at a temperature of 25 ± 2 °C. An aquarium air pump (VENUS AQUA; AP-208, 2.5 W) with a flow rate of 3 L/min was used to supply ambient air and intermingling in the microalgae culture pond. The schematic representation of microalgae culture in HRAP using municipal wastewater has shown in Fig. 1. The microalga *C. sorokiniana* used in the experiment was initially adapted in sterile municipal wastewater for 7 days. Then, adapted microalgae cells (logarithmic phase) were used to inoculate in the microalgae culture pond ($OD_{750\ nm}$ = ~ 0.200) to cultivate for 14 days.

2.3. Microalgae biomass growth, biochemical compositions, and pigments analysis

The growth of the microalgae *C. sorokiniana* biomass in municipal wastewater and control media (BBM) was measured in terms of optical density at 750 nm at regular 2-day intervals. The microalgae biomass was harvested in the stationary phase (day 14) to estimate the biochemical compositions (total carbohydrates, total proteins, and total lipids). The dry cell weight (dcw) of the microalgae biomass was estimated by the gravimetric technique. Total carbohydrates, total proteins, and total lipids were assessed by the phenol sulfuric acid method, the Bradford test, and the modified Bligh and Dyer method, respectively (Bligh and Dyer, 1959; Bradford, 1976; Masuko et al., 2005). In the lipid extraction process, the freshly collected microalgae biomass was mixed with the solvents methanol, chloroform, and water (in a ratio of 2: 1: 0.8) and subsequently followed by ultrasonication for 10 min to disrupt the cells. Then, the sample was applied for centrifugation for 5 min at 10,000 rpm. After centrifugation, the supernatant was separated and mixed with a 0.1% NaCl solution, mixed vigorously, and applied again for centrifugation. The lower chloroform layer containing microalgae lipids were removed by pipetting. The total biomass productivity was determined using the equation:

$$\textit{BiomassProductivity}\quad (mgL^{-1}Day^{-1}dcw) = \frac{B_f - B_i}{D} \tag{1}$$

Where 'B_f' is the biomass harvested at the end of cultivation, 'B_i' is the initial biomass at the start of cultivation, and 'D' is the total number of the day of biomass cultivation.

Photosynthetic pigments (Chlorophyll 'a', chlorophyll 'b', and carotenoids) were quantified by preparing methanolic extract and measuring the absorbance at 470 nm, 652.4 nm, 665.2 nm, and 750 nm (to exclude impurities) (Lichtenthaler, 1987). The pigment determination was calculated with the equations:

$$\textbf{Chlorophyll 'a' (Chl 'a'; μg/ml)} = \textbf{16.72 } A_{665.2} - \textbf{9.16 } A_{652.4} \tag{2}$$

$$\textbf{Chlorophyll 'b' (Chl 'b'; μg/ml)} = \textbf{34.09 } A_{652.4} - \textbf{15.28 } A_{665.2} \tag{3}$$

$$\textbf{Carotenoids (μg/ml)} = (\textbf{1000 } A_{470} - \textbf{1.63 Chl 'a'} - \textbf{104.9 Chl 'b'})/221 \tag{4}$$

Where '$A_{665.2}$' is the absorbance at 665.2 nm, '$A_{652.4}$' is the absorbance at 652.4 nm, and 'A_{470}' is the absorbance at 470 nm.

2.4. Hydrothermal carbonization-co-liquefaction of microalgae biomass (oiled/de-oiled)

The microalgae biomass harvested in the stationary phase and the

biomass after lipid extraction (oiled/de-oiled) were used for the hydrothermal carbonization-co-liquefaction (HTCL) process. HTCL processes were carried out in stainless steel (SS-316) reactors with an internal dimension of length (17.5 cm) and diameter (1.5 cm). Dry and powdered microalgae biomass (oiled/de-oiled), alkaline catalyst sodium carbonates (Na_2CO_3), and Milli-Q water were used by weight. % ratio 1.0: 0.1: 6.0 for reaction in a muffle furnace (ACMAS Technologies Pvt. Ltd.) with a heating rate of 5 °C/min. The operating temperature was used at 400 °C (slightly above the supercritical temperature) for 6 h. After the HTCL reaction, the reactors were cooled to room temperature, and then the liquid and solid phases of HTCL products were separated. The dichloromethane solvent was added to the liquid phase to separate the bio-oils from the aqueous layer. The dichloromethane solvent was then evaporated by a rotary evaporator to obtain pure bio-oils. The solid phase of the HTCL products was washed with acetone to separate acetone soluble bio-oils. After evaporating the acetone, the acetone soluble bio-oil was mixed with the dichloromethane soluble bio-oil for analysis. The obtained solid HTCL products were washed with Milli-Q water and dried in a hot air oven at 60 °C. The bio-char obtained was ground into fine powder for heavy metal remediation experiments. The schematic representation of HTCL of microalgae biomass after lipid extraction (oiled/de-oiled) has shown in Fig. 1. The bio-chars and bio-oils yield were calculated using the equations:

$$\boldsymbol{Bio-oil}(\%) = \frac{\boldsymbol{B_{of}}}{\boldsymbol{W}} \times \mathbf{100} \quad (5)$$

$$\boldsymbol{Bio-char}(\%) = \frac{\boldsymbol{B_{sp}}}{\boldsymbol{W}} \times \mathbf{100} \quad (6)$$

Where 'B_{of}' is the dried weight of bio-oils organic fractions, 'B_{sp}' is the dried weight of bio-chars solid phase, and 'W' is the dry cell weight of microalgae biomass used for the HTCL process.

2.5. Characterization and analysis of bio-char and bio-oil

The structural composition, phase purity, lattice parameter, and crystalline size of the prepared bio-chars (MB-OB and MB-DOB) were analyzed by powder X-ray diffractometer (X'Pert PRO, PAN-alytical) with Cu Kα radiation (λ = 1.5406 Å) in the range 10–80° with the step size of 0.015°. LASER Raman Spectroscopy (RENISHAW in Via Raman confocal microscope system) was performed at an excitation wavelength of 785 nm. The infrared spectra (400–4000 cm^{-1}) of the microalgae biomass (M-OB and M-DOB) and the bio-chars (MB-OB and MB-DOB) were recorded using the Fourier transform infrared spectrometer (Thermo Nicolet Model 6700) using the KBr pellet technique. Elemental analysis of microalgae biomass and bio-chars was carried out using Semi-macro Elemental analyzers (CHNS; carbon, hydrogen, nitrogen, sulphur) (Vario EL cube V3.1.8). The surface morphologies of the microalgae biomass and the bio-chars were characterized by the scanning electron microscope (Hitachi S-3400N). Measurements of the surface area of the microalgae biomass and the bio-chars were performed using Brunauer–Emmett–Teller (BET) with nitrogen adsorption-desorption apparatus (Micrometrics Instruments USA–ASAP2020). The ^1H NMR spectra of bio-oils were recorded using 400 MHz Fourier Transform - Nuclear Magnetic Resonance (Bruker Advance-II).

2.6. Multiple heavy metals remediation of bio-char

The multiple heavy metal solution was prepared by dissolving the heavy metal salts viz. Copper(II) sulfate pentahydrate ($CuSO_4.5\ H_2O$), nickel(II) nitrate hexahydrate ($Ni(NO_3)_2.6\ H_2O$), cobalt(II) nitrate hexahydrate ($Co(NO_3)_2.6\ H_2O$) and cadmium chloride hemi(pentahydrate) ($CdCl_2.2.5\ H_2O$) in the concentration of 25 mg/L each in Milli-Q water. The effect of the pH for the removal of multiple heavy metals was investigated in the range 2-6.18. The prepared microalgae bio-chars (MB-OB and MB-DOB) were used for the remediation of multiple heavy metals in batch experiments at room temperature. The bio-char concentration (250 mg) was added to 100 ml of multiple heavy metal stock solutions in the Erlenmeyer flask and placed on a rotary flask shaker at 200 rpm. The schematic representation of multiple heavy metal remediation using microalgae bio-chars and possible mechanisms have illustrated in Fig. 1. The suspension of bio-char and multiple heavy metals solutions were removed from the shaker at different time intervals, viz. 10, 30, 60, 90, 120, 180, 240, 480, 720, and 1440 min, and centrifuged to separate the solid bio-char from the metals solution phase. The solution phase was taken to analyze the remaining concentration of multiple heavy metals via the Ion Chromatography System (ICS). The adsorptions of multiple heavy metals in bio-chars were calculated using the following equation:

$$\boldsymbol{Heavymetalsremediation}(\%) = \frac{\boldsymbol{C_i} - \boldsymbol{C_f}}{\boldsymbol{C_i}} \times \mathbf{100} \quad (7)$$

Where, 'C_i' is the initial concentration of the heavy metals in the solution and 'C_f' is the final concentration of the heavy metals in the solution after remediation with bio-chars.

2.7. Statistical analysis

All the experiments of microalgae cultivation (biomass growth and biochemical compositions) and the adsorptions of multiple heavy metals in bio-chars were performed in triplicate (n = 3), and variability are presented as mean ± standard deviations (SD). The microalgae growth curve, histogram, and spectroscopic data were plotted using OriginPro 8.5 software.

3. Results and discussion

3.1. HRAP performance for municipal wastewater mitigation, biomass productivity, and biochemical compositions

The physicochemical parameters of the collected MWW indicated non-permissible levels of alkalinity, hardness, TKN, TP, BOD, and COD that require mitigation (Table S1). Cultivation of *C. sorokiniana* UUIND6 in MWW has demonstrated complete elimination of foul smell in 5 days and color changed from yellowish-brown to clear in 14 days. In the MWW treated with microalgae at 14 days, the reduction of the high nutrient load was observed in terms of TKN (~95%) and TP (~97%) (Table S1). Microalgae have shown the ability to metabolize inorganic and organic nitrogen for growth, although it preferably uses NH_4^+ due to the lower energy requirement followed by NO_3^- and NO_2^- (Kadir et al., 2018). In addition, unsterilized MWW that has indigenous bacteria nitrifies NH_4^+ to NO_3^- by establishing a synergistic relationship to assimilate nitrogen by microalgae in HRAP (Hernández-prieto et al., 2016). Similarly, phosphorus assimilation has also been reported, since it is a vital micronutrient in cell survival and development (Arora et al., 2015). Furthermore, the synergistic effect of microalgae and indigenous MWW bacteria leads to the elimination of BOD (~82%), COD (~83%), and TOC (~71%) (Table S1). MWW bacteria use photosynthetic O_2 to break down dissolved organic compounds and release nitrogen, phosphorous, and CO_2 to assimilate by microalgae (Nirmalakhandan et al., 2019). Microalgae have been reported to release small organic molecules (e.g. glycolic acid), predominantly in the stationary phase, therefore, a complete reduction in organic content was not observed (Mulders et al., 2014). Increasing the pH from 7.72 (before treatment) to 8.84 (after treatment) designates microalgae as a dominant species in HRAP since the growth of microalgae increases the pH of the media (Table S1). Moreover, improvement in DO (~90%) after MWW treatment reveals oxygenation in HRAP due to intensive photosynthesis of microalgae (Park et al., 2011).

The nutritional composition of the culture media directly influences the growth rate, the productivity of the biomass, and the biochemical

Table 1
CHNS composition of microalgae biomass and bio-chars.

S. No.	Sample	N [%]	C [%]	H [%]	S [%]	C/N ratio	C/H ratio
1.	M-OB	5.934	31.677	5.263	1.234	5.338	6.018
2.	M-DOB	5.945	33.567	5.706	1.190	5.646	5.882
3.	MB-OB	0.954	9.654	0.366	2.080	10.114	26.411
4.	MB-DOB	0.555	5.015	0.265	1.820	9.041	18.897

compositions of the microalgae. In this study, the effect of MWW on the growth and biochemical compositions of *C. sorokiniana* was determined after 14 days and compared with the control media (BBM). Microalgae have demonstrated good adaptability in MWW with ~42% increased dry cell weight (dcw) (880.594 ± 14.37 mg/L) in MWW compared to control media (622.167 ± 12.21 mg/L) (Fig. S1). The productivity of the microalgae biomass was determined in 14 days of culture as ~46% higher in MWW (58.478 ± 0.88 mg/L/D dcw) than BBM (40.142 ± 0.84 mg/L/D dcw). The increase in biomass growth and productivity indicates the efficient usage of available nutrients in MWW, which was also evident in terms of the reduction of TKN, TP, and TOC (Table S2). Compared to control media, MWW consisted of numerous organic carbons (e.g. acetate, glycerol, and glucose) that lead to the mixotrophic behavior of *C. sorokiniana* and allow the use of inorganic carbon (CO_2) and organic carbon (TOC in MWW) to express superior biomass growth and productivity compared to BBM (Arora et al., 2020).

The biochemical composition of *C. sorokiniana* grown in HRAP+MWW and control media (BBM) was analyzed in terms of total carbohydrates, total proteins, and total lipids (Fig. S2 and Table S3). A substantial increase in total carbohydrates (~ 9%) and total lipids (~25%) was recorded for the biomass of microalgae grown in MWW compared to BBM. Increased expression of the ribulose 1,5 bisphosphate carboxylase/oxygenase (RuBisCo) large subunit (rbcL gene), acetyl-CoA carboxylase subunit (accD), and acc1 gene have been reported to trigger lipid accumulation in stationary phase under mixotrophy (Wan et al., 2011). In addition, the stress environment occurs due to the existence of toxic organic compounds and heavy metals in MWW that initially accumulate carbohydrates followed by lipids (Arora et al., 2019). However, the total protein content decreased ~ 16% in the biomass of *C. sorokiniana* grown in HRAP+MWW compared to control media, which could be due to the un-regulation in carbohydrate and lipid biosynthesis.

Photosynthetic pigments (such as chlorophyll a, chlorophyll b, and carotenoids) serve as an indicator of the presence of microalgae as the main organism in HRAP. Microalgae grown in MWW have shown an apparent increase in chlorophyll a and chlorophyll b ~35% in microalgae grown in MWW in comparison to control media revealed enhanced photosynthesis in HRAP with dominant microalgae cells over the indigenous MWW bacterial population (Fig. S3 and Table S4). In addition, a ~59% increase in total carotenoids was observed in MWW cultured microalgae cells compared to the control. The increase in photosynthetic pigments grown in HRAP+MWW could be due to the activation of mixotrophic behavior that reduces photo-inhibition due to less susceptibility of light stress to microalgae cells. Furthermore, mixotrophy supports the significant reuse of CO_2 produced from the metabolism of the respective carbon source (Vonshak et al., 2000).

3.2. Elemental (CHNS) analysis of microalgae biomass and bio-chars

The elemental compositions (CHNS) of the microalgae biomass (M-OB and M-DOB) and the prepared bio-char (MB-OB and MB-DOB) are shown in Table 1. CHNS analysis revealed that the C/H ratio in de-oiled microalgae biomass (M-DOB) has decreased compared to oiled biomass (M-OB) due to lipid extraction. Bio-char prepared from oiled microalgae biomass (MB-OB) has a high C/H ratio. The low C/H ratio of bio-char prepared from de-oiled microalgae biomass (MB-DOB) is in agreement with the C/H ratio of de-oiled microalgae biomass. The low C/H ratio attests to the efficient creation of a highly disordered graphitic structure in MB-DOB (as earlier described in XRD and Raman analysis).

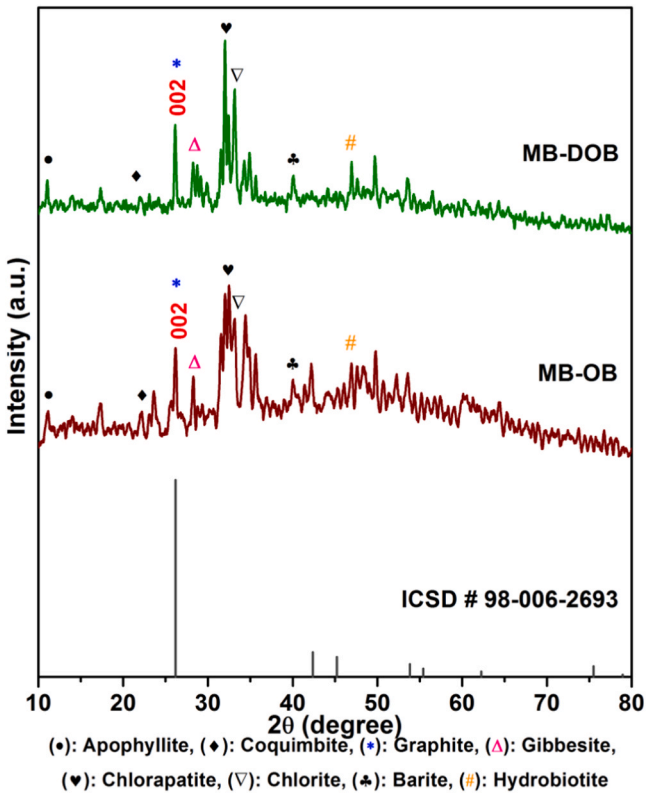

Fig. 2. XRD pattern of microalgae bio-chars obtained from oiled and de-oiled biomass.

3.3. Powdered XRD of microalgae bio-chars

The X-ray diffraction pattern of the microalgae bio-char of oiled biomass (MB-OB), de-oiled biomass (MB-DOB), and the ICSD standard reference is shown in Fig. 2. X-ray diffraction spectral analysis revealed that the evolution of various peaks corresponds to the wide range of crystalline and inorganic mineral materials. Several peaks have been found to overlap, establishing the grouping of more than one possible peak. The prominent sharp diffraction peak evolved in the oiled and de-oiled microalgae bio-chars at 26.1° (0 0 2) ascribed to the graphite 2H indexing planes, indicating the carbon hexagonal crystal system (ICSD Card No.: 98-006-2693) (Seehra et al., 2015). Another sharp diffraction peak with high intensity at 32.0° corresponds to the structural composition of chlorapatite in microalgae bio-char. Chlorapatite formation is due to the reaction of the Na_2CO_3 catalyst used with the microalgae biomass minerals during the hydrothermal liquefaction reaction (Deng et al., 2020). A number of additional diffraction peaks with relatively lower intensities at 11.1°, 21.9°, 28.4°, 33.1°, 40.1°, and 46.8° were also assigned to apophyllite, coquimbite, gibbsite, chlorite, barite, hydrobiotite, respectively. It is also observed that numerous diffraction peaks and corresponding intensities were reduced along with slightly higher noise signals and background (Waqas et al., 2018). The variations in the diffraction peaks represent the disintegration of minerals during the hydrothermal liquefaction reaction and the formation of new components. The XRD analysis of the microalgae bio-chars also notices the presence of a wide range of mineral constituents such as Al, C, Na, Si, Ca, Mg, Cl, K, Fe, and S. The EDS spectra revealed the existence of different chemical elements with different evolved peaks in the sample of

Table 2
Crystallite sizes of structural compositions in microalgae bio-chars.

S. No.	Sample	Structural Composition	Peak Position (2θ)	FWHM	Crystallite Size (nm)
1.	MB-OB	Graphitic (0 0 2)	26.34°	175.62	4.65
2.		Chlorapatite	32.22°	184.90	4.47
3.	MB-DOB	Graphitic (0 0 2)	26.16°	57.98	14.07
4.		Chlorapatite	32.04°	57.98	14.27

inhomogeneous bio-chars (mainly strong peaks for C, O, P and Ca) (Fig. S4). It is also observed that the hydrothermal liquefaction reaction affects the structurally, chemical, and mineralogical heterogeneity of the microalgae bio-char (Yuan et al., 2011; Ahmad et al., 2017).

The crystallite size of the microalgae bio-chars obtained from oiled and de-oiled biomasses are shown in Table 2. The crystallite size of the graphite 2H indexing planes was calculated using the Debye-Scherrer equation [crystallite size (D) = Kλ/ (β cos θ)] as 4.65 nm and 14.07 nm using the peak positions 26.34° (0 0 2) and 26.16° (0 0 2) in the bio-chars of oiled and de-oiled biomass, respectively (Jaiswal et al., 2018). The crystallite size of chlorapatite was calculated 4.47 nm and 14.27 nm using the highest intensity peaks at the peak positions 32.22° and 32.04° in the bio-chars of oiled and de-oiled biomass, respectively. Smaller crystallite sizes of graphite 2H and chlorapatite in the bio-char of oiled biomass indicate the amorphous presence. While the higher crystallite sizes in the bio-char of de-oiled biomass endorse the higher crystalline phase. Here, the higher C/N and lower C/H ratio of the de-oiled biomass (M-DOB) (as observed in the CHNS analysis) plays an essential role in the creation of bio-char with a high crystalline structure. The size of crystallite also helps to understand the size of the bio-char grains/particles (Tyler and Wooding, 1958; Wang et al., 2007).

3.4. Raman spectroscopy of microalgae biomass and bio-chars

The Raman spectra of the microalgae biomass (M-OB and M-DOB) and the prepared bio-char (MB-OB and MB-DOB) are presented in Fig. 3. There is no band appearance in the microalgae biomass (M-OB and M-DOB). While the microcrystalline structure of the bio-chars revealed the appearance of two broad bands centered at 1351 cm^{-1} (D band) and 1585 cm^{-1} (G band) in MB-OB and 1335 cm^{-1} (D band) and 1580 cm^{-1} (G band) in MB-DOB, demonstrating the amorphous structure. The D band structures are interpreted as aromatic clusters having more than 6 rings and a higher FWHM suggests a highly amorphous nature of the carbon structure, while the G band attributes to the E_{2g} symmetry of the graphite layers in the bio-chars (Maliutina et al., 2018; Sudhakar et al., 2018). G bands in microalgae bio-chars conform to sp^2 hybridized C atoms, and D bands originate as defects generated in the carbon lattice. The extent of defects in bio-chars has been quantified by the intensity ratio of D band to G band (I_D/I_G) (Table S5) (Sudhakar et al., 2017; Yang et al., 2019). The I_D/I_G ratio of MB-OB and MB-DOB is 0.919 and 1.053, respectively which specifies the large size of the sp^2 in-plane carbon domains. The increase in the I_D/I_G ratio of MB-DOB indicates the highly disordered graphitic structure in the de-oiled biomass, which is due to the high C/N and low C/H ratio (as seen in the CHNS analysis; Table 1). The strong D band of MB-DOB has been accompanied by defects in most of the graphitic carbon due to the appearance of functional groups such as carbonyl, hydroxyl, and epoxy (Yao et al., 2018). The appearance of carbonyl functionalities in bio-chars denotes the competence to adsorb heavy metal ions on surfaces.

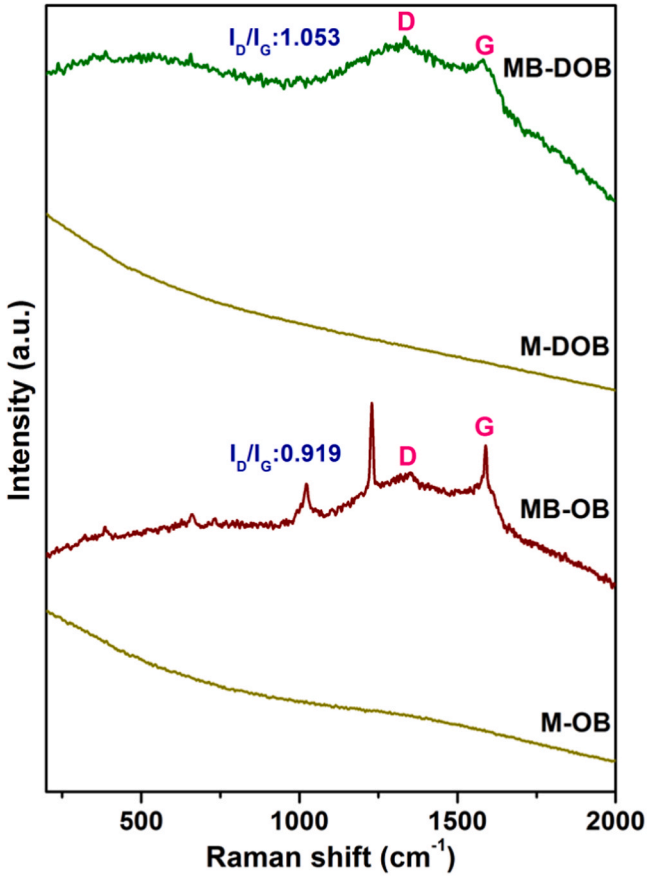

Fig. 3. Raman spectra of microalgae biomass and obtained bio-chars.

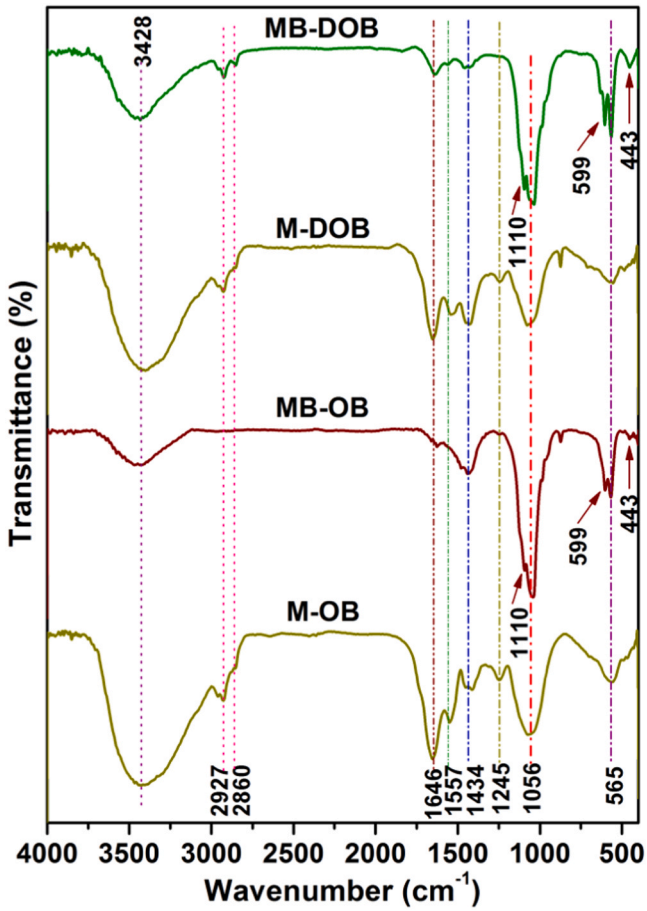

Fig. 4. FT-IR spectral peaks of microalgae biomass and obtained bio-chars.

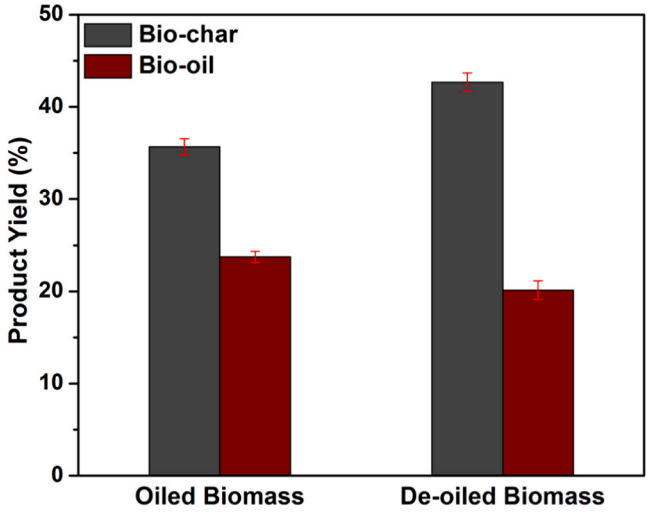

Fig. 5. HTCL product yield of microalgae bio-chars and bio-oils.

3.5. FTIR spectroscopy of microalgae biomass and bio-chars

FT-IR spectroscopy was performed to recognize the functional groups present in the oiled/de-oiled microalgae biomass and bio-chars. The characteristic wavenumbers and approximate vibrational mode assignments are shown in (Fig. 4 and Table S6). The absorption peak at 443 cm^{-1}, 565 cm^{-1}, and 599 cm^{-1} corresponds to the stretching vibration of halocarbons such as organo–F, organo–Cl, organo–Br, and organo–I. The distinctive peak vibrations at 3428 cm^{-1} and 1646 cm^{-1} correspond to the stretching vibrations of O–H and C═O, respectively endorsing carboxylic (–COOH) functional groups (Huff and Lee, 2016). The presence of carboxylic functionalities in the bio-chars denotes the competence to adsorb heavy metal ions on surfaces. The reduction in the intensity of carboxyl functional groups has been observed for bio-chars, possibly due to the volatilization of carboxyl functionality in hydrothermal pyrolysis of microalgae biomass. The decrease in H/C atomic ratios (as observed in the CHNS analysis) supports this hypothesis. However, the reduction in the amount of negatively charged surfaces of microalgae bio-chars associated with oxygen-containing functionalities, such as –COOH, –COH and –OH supports the increase in pH to improve adsorption sites for heavy metal ions (Michalak et al., 2019; Zhao et al., 2019). The peak vibration at 2927 cm^{-1} corresponds to the stretching vibrations of the C–H band of cellulose and hemicellulose reduced in the bio-chars. Also, the reduction in the intensity of the –OH groups at 3428 cm^{-1} revealed the decomposition of the phenolic and alcoholic functionalities, while the reduction of aliphatic C−H groups at 2860 cm^{-1} and 2927 cm^{-1} indicated that the methyl groups were eliminated from the aromatic rings (Yuan et al., 2015). The peak vibration at 1056 cm^{-1} corresponded to the C–O band of methoxy functional groups reduced due to the thermal decomposition, cleavage of organic groups and evolution of gases. The peak vibrations corresponding to the nitrogen-containing amine/amide functional groups at 1646 cm^{-1} and 1245 cm^{-1} were cracked at the temperatures and pressures of hydrothermal pyrolysis. However, the pyridinic, pyrrolic and quaternary structures conforming generation of graphitic configurations were retained in bio-chars (demonstrated by XRD and Raman analysis). The reduction in aromatic substituents and disintegration of heteroatom functionalities signifies the production of gases that contain oxygen and nitrogen (Debono and Villot, 2015).

3.6. The yield of microalgae bio-chars and bio-oils

The yield of the microalgae bio-char and the bio-oil of the microalgae biomass (M-OB and M-DOB) are presented in Table S7 and Fig. 5. The development of bio-char from de-oiled microalgae biomass is higher (42.66 ± 1.0) than oiled microalgae biomass (35.66 ± 0.9), whereas bio-oil generation is higher (23.73 ± 0.6) in oiled microalgae biomass. Here, the higher bio-oil generation is supported by the higher C/H ratio of the oiled microalgae biomass, while the lower C/H ratio supports the formation of bio-char.

3.7. Scanning electron microscopy of microalgae biomass and bio-chars

Fig. 6 illustrates the representative scanning electron micrograph of microalgae oiled/de-oiled biomass and prepared bio-char. The surface morphology of the microalgae oiled biomass (M-OB) represents intact spherical shapes and smooth surfaces (Fig. 6a and b). The surface structure of bio-char prepared from microalgae oiled biomass (MB-OB) exhibited a mutilated shape and a deformed surface due to the volatilization of organic components (Fig. 6c and d) (Usman et al., 2015). The morphology of microalgae de-oiled biomass (M-DOB) has shown cracked and fragmented forms with irregular surface structures due to the disruption of the cell walls in lipid extraction (Fig. 6e and f). The bio-char prepared from microalgae de-oiled biomass showed flakes like structures and micro-rods (Fig. 6g and h). A significant transformation of M-DOB resulted in bio-char of flakes like structure and micro-rod, due to the volatilization process of organic materials and thermal pyrolysis of cell debris. The irregular flakes structure of the MB-DOB was generated at a high temperature due to the condensation of organic hydrocarbon materials as tars and the successive disintegration of the products in carbonization (Waqas et al., 2018). The electron micrographic characteristics of bio-char for heterogonous mineralogical compositions coincide with the XRD and Raman structural analysis.

3.8. BET surface area analysis of microalgae biomass and bio-chars

The Brunauer–Emmett–Teller (BET) surface area of microalgae oiled/de-oiled biomass and the prepared bio-chars are shown in Table S8. The BET surface area of M-OB and M-DOB was found to be 1.544 ± 0.047 m^2/g and 1.663 ± 0.026 m^2/g, respectively. A noteworthy increase in the surface area of de-oiled biomass was observed, which could be due to the mutilated and fragmented cellular structure of microalgae biomass. Noteworthy, the surface area of the bio-chars increased during the hydrothermal carbonization-co-liquefaction process for MB-OB and MB-DOB as 14.759 ± 0.070 m^2/g and 15.187 ± 0.079 m^2/g, respectively. The increase in surface area of prepared microalgae bio-char is due to the thermal pyrolysis at high temperatures (Cao and Harris, 2010). The remarkable high surface area of MB-DOB obtained from microalgae de-oiled biomass could be due to the creation of micro-rods and flakes like morphology of graphitic bio-char (as seen in SEM).

3.9. ^{1}H-NMR spectroscopy of microalgae bio-oils

Fig. 7 illustrates the ^{1}H NMR spectra of microalgae bio-oils (BO-OB and BO-DOB) obtained from the HTCL of microalgae biomass (M-OB and M-DOB). The spectra have exposed the major variances in the general chemical characteristics of the bio-oils. The maximum upfield signals of the bio-oils spectra (BO-OB and BO-DOB) in the regions 0.8–1.5 ppm signifies the aliphatic protons attached to carbon atoms, at least two bonds eliminated from a C═C or heteroatoms (O or N). It was mostly occupied in the regions and indicates superior aliphatic components for bio-oils (Mullen et al., 2009). Its higher value in the BO-OB corresponds to the hydrothermal liquefaction product of the hydrocarbon components of the microalgae oiled biomass. Thus, it advocates that aliphatic hydrocarbon chains comprising of two or more bonds are more dominant in M-OB bio-oils than M-DOB. Similarly, it also predicts the carbon contents and, subsequently, the calorific values of the bio-oils (Mullen et al., 2009).

The subsequent integration signals in the 1.5–2.5 ppm region signify

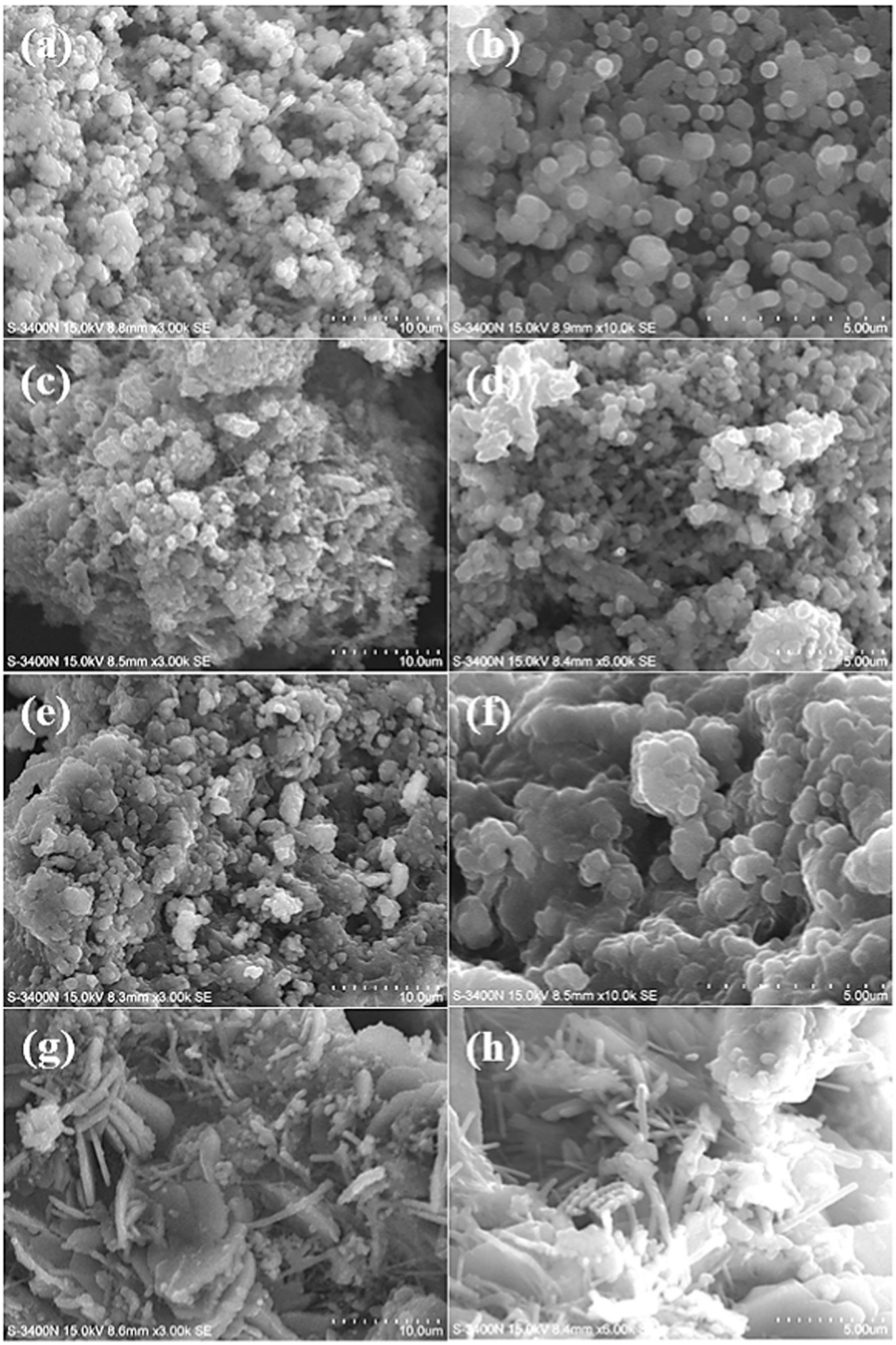

Fig. 6. Scanning electron micrograph of M-OB (a and b), MB-OB (c and d), M-DOB (e and f), and MB-DOB (g and h).

protons in aliphatic carbon atoms that may be bonded to a C═C (aromatic or olefinic) or two bonds of a heteroatom. Bio-oil of de-oiled microalgae biomass (BO-DOB) has shown rich in these protons in this spectral region, while bio-oil of oiled biomass (BO-OB) has the least amount of these protons in this category. This recommends that the aliphatic portions of the molecules, even those attached to aromatic portions or close to the heteroatoms, are more dominant for bio-oils that contain more energy (Boateng et al., 2007). The water molecules in bio-oils can probably also resonate in this region, but as we described in the experimental section, bio-oils were collected using organic solvents (CH_2Cl_2 and $(CH_3)_2CO$) and analyzed with organic solvents ($CDCl_3$), water signals are insignificant features in spectra (Mullen et al., 2009).

The next region including downfield from 2.5 to 8.0 ppm consist of protons of the carbon atoms next to aliphatic alcohol or ether, or a methylene group that binds two aromatic rings (2.5–4.5 ppm), the protons of the aromatic ether, and many of the hydrogen atoms of carbohydrate-like molecules (4.5–6.0 ppm), and the hydrogen atoms in benzenoids and heteroaromatics that contain small amounts of O and N (6.0–8.0 ppm) in both bio-oils (Mullen and Boateng, 2008). In general, the ^{1}H NMR analysis demonstrates that aliphatic protons are mostly prevailing for bio-oils derived from microalgae oil biomass, whereas protons proximal to heteroatoms (alcohols, carbohydrates) are

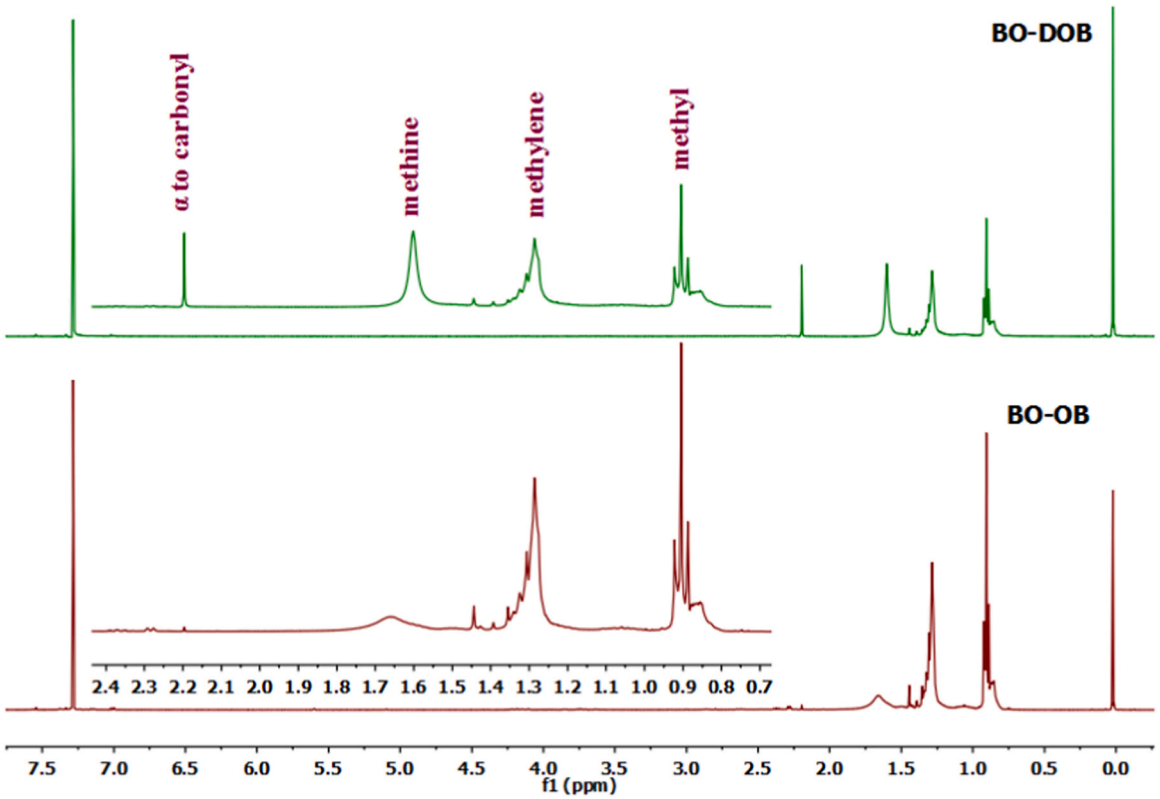

Fig. 7. ^{1}H NMR spectra of bio-oils obtained from microalgae oiled/de-oiled biomass.

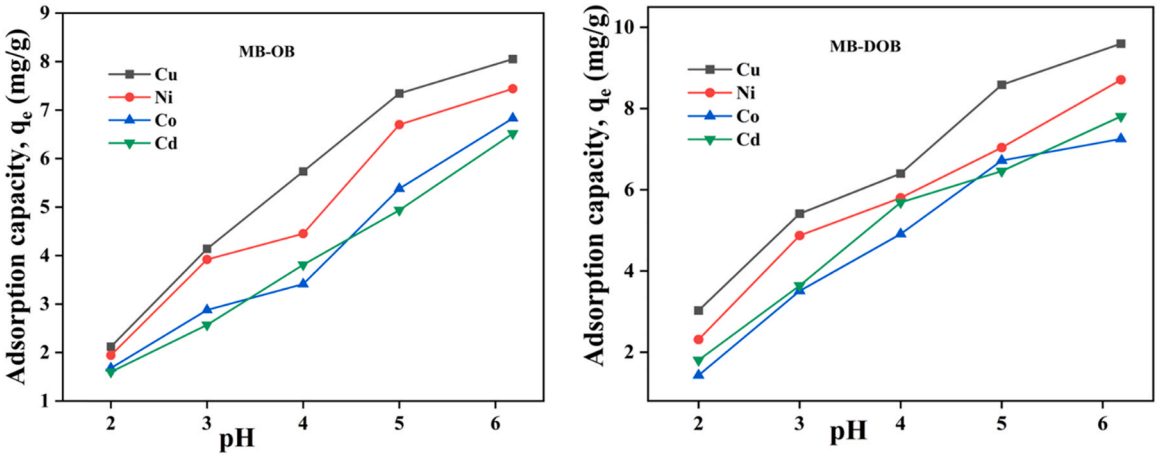

Fig. 8. Effect of pH on the adsorption capacity of MB-OB and MB-DOB on multiple heavy metal ions.

extremely intense in bio-oil of de-oiled biomass.

3.10. *Effect of pH on the adsorption of multiple heavy metals*

The pH of the adsorption solution exerted a marked impact on the adsorption of heavy metals by adsorbents. The pH effect was carried out with a 100 ml mixture of multiple heavy metal ions (25 ml each, 25 mg/L) with 500 mg adsorbent. Fig. 8 displays the effect of solution pH (2–6.18) on the adsorption capacity and Fig. S5 displays the % removal of multiple heavy metals on MB-OB and MB-DOB. Data indicates that the adsorption capacity increased continuously with increasing solution pH and was poorest when the solution pH was 2. The adsorption capacity of MB-OB and MB-DOB for the Cu(II), Ni(II), Co(II), and Cd(II) at pH 2 was 2.12/1.94/1.68/1.6, and 3.02/2.31/1.43/1.80 mg/g, which was increased up to 8.05/7.44/6.83/6.51 and 9.59/8.70/7.25/7.78 mg/g at the solution pH 6.18, respectively. The low adsorption capacity at lower pH for the heavy metal ions was due to the protonation of surface functional groups of MB-OB and MB-DOB which produce electrostatic repulsion between free heavy metal ions and positively charged surface functional groups as earlier reported in the literature (Xiao et al., 2017; Verma et al., 2020; Zhang et al., 2020). Also, at lower pH, triggers competition for adsorption sites between heavy metal ions and hydrogen ions occurs which leads to low adsorption capacities. As the solution pH increases, the competition between heavy metal ions and hydrogen ions decreases and increasing the adsorption capacity of heavy metal ions. The point of zero charges (Pzpc) of MB-OB and MB-DOB is less than 2.6 and the surface of the MB-OB and MB-DOB become deprotonated above this value (pH>Pzpc). Thereby, enhances electrostatic attraction

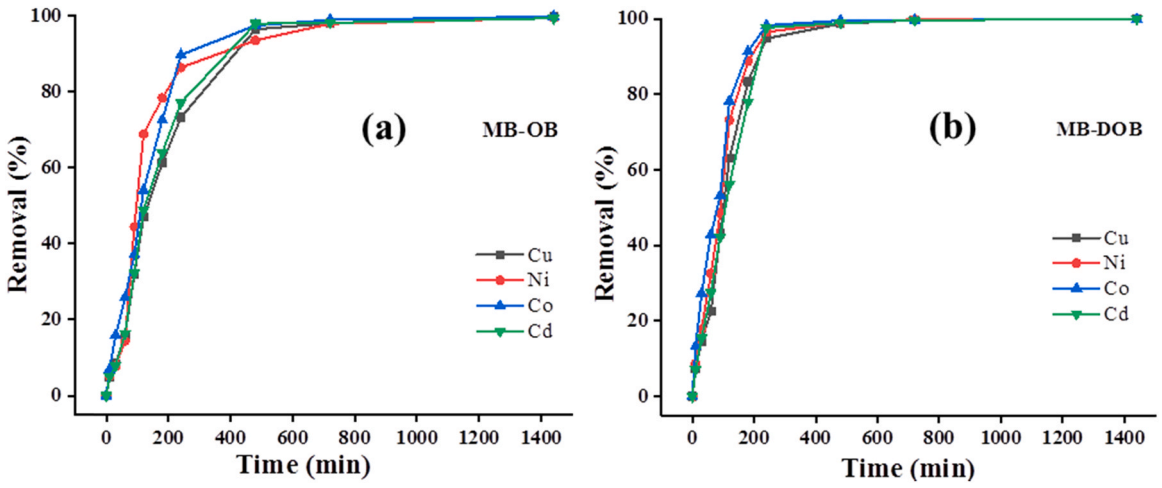

Fig. 9. Multiple heavy metals remediation efficiencies of bio-chars.

between the surface of MB-OB and MB-DOB, and heavy metal ions. When the pH of the solution was greater than 6.18, a white precipitate of the cadmium hydroxide was formed (Park et al., 2017), which affect the adsorption capacity of the adsorbents. Therefore, the initial solution pH was chosen 2−6.18 for the pH effect and pH 6.18 was chosen as an optimal pH for further experiments.

3.11. Effect of contact time between the bio-char adsorbents and heavy metals in multiple heavy metals remediation system

Fig. 9 shows the removal efficiency of multiple heavy metals of bio-char obtained from microalgae oiled/de-oiled biomass. Statistics (mean ± SD) for the remediation efficiency of multiple heavy metals at 60, 120, 240, 720, and 1440 min are given in Table S9. The maximum HMR was observed as 14.40 ± 1.7–25.84 ± 1.8% and 22.55 ± 1.3–42.88 ± 1.5% in 60 min, 47.00 ± 1.5–68.84 ± 3.3% and 56.24 ± 1.0–78.24 ± 1.2% in 120 min, 73.24 ± 1.2–89.68 ± 1.4% and 94.86 ± 1.4–98.34 ± 1.4% in 240 min, 97.88 ± 0.6–98.92 ± 0.7% and 99.67 ± 0.3–99.89 ± 0.2% in 720 min, 99.36 ± 0.2–99.80 ± 0.4% and 99.99 ± 0.1–100.00 ± 0.0% in 1440 min, of MB-OB and MB-DOB, respectively, for the multiple heavy metals solution (Cu(II), Ni(II), Co (II), and Cd(II)). The results obtained revealed that the efficiency of total HMR of MB-OB was 18.13 ± 1.6%, 54.71 ± 2.1%, 81.60 ± 1.6%, 98.25 ± 0.2%, and 99.57 ± 0.4% in 60, 120, 240, 720, and 1440 min, respectively, whereas the efficiency of total HMR of MB-DOB was 31.36 ± 1.4%, 67.68 ± 0.7%, 96.86 ± 1.4%, 99.74 ± 0.1%, and 99.99 ± 0.0%, respectively. The efficiency of HMR was increased due to the larger BET surface area and surface functionalities such as carbonyl, hydroxyl, and epoxy in graphitic MB-DOB (Liu et al., 2015). The highly disordered flakes like morphology of graphitic MB-DOB were attested by XRD, Raman, and SEM analysis. Multiple heavy metals remediation has been endorsed as an integrated approach of accessible functional groups and surface phenomena on bio-char via physical adsorption, precipitation, surface complexion, electrostatic interaction, and ion exchange. The graphitic bio-chars obtained from the microalgae biomass are the characteristic inhomogeneous structure due to the existence of the wide range of crystalline and inorganic mineral materials. The compositional structure of microalgae bio-chars can instigate the heavy metals removal with an integrated approach of accessible functional groups and surface phenomena on bio-char. The possible heavy metals remediation mechanism of bio-char can possess different approaches. Adsorption phenomenon is a mass transfer process to transfer the heavy metals from the multiple heavy metal solution to the solid bio-chars, and bound via physical and/or chemical interactions. The phenomenon of precipitation of removal of heavy metals is due to the impact of the addition of

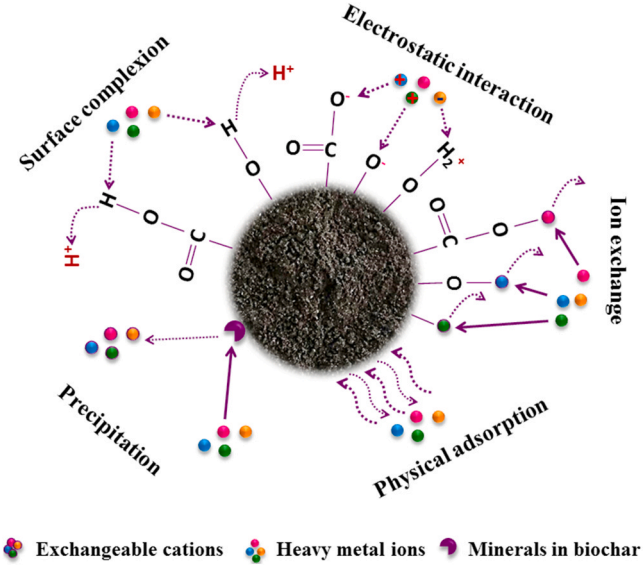

Fig. 10. Schematic representation of mechanisms for multiple heavy metals remediation.

alkali (e.g. Caustic or lime) to adjust the pH of the solution of multiple heavy metals to the point of minimum solubility of the exposed metals. The formation of the surface complex for the removal of heavy metals is due to the formation of coordination bonds between the donor (i.e., ligands) and the acceptor (i.e., metal ions). The existence of functionalities (such as carboxylic, hydroxyl and amine) on the surface of the bio-chars accelerates the formation of the complex due to the transfer of electrons at the external energy level with the center of the metal ions. The electrostatic interaction phenomenon plays a significant role in the adsorption of heavy metals from the multiple heavy metal solution using electrostatic forces on the surface active sites. The ion exchange phenomenon is a reversible chemical reaction, in which ions (an atom or molecule having lost or gained an electron to acquire electrical charges) from the multiple heavy metal solution can be exchanged with alike charged ions available on bio-chars (Yang et al., 2019). The possible heavy metals remediation mechanism is illustrated in Fig. 10.

To determine the equilibrium, the effect of contact time between the adsorbent (MB-OB and MB-DOB) and heavy metals in multiple-metal systems (Cu(II), Ni(II), Co(III), and Cd(II)) was investigated. For that, experiments were carried out by taking 100 mg of multiple heavy metals solution (each 25 mg) with 250 mg bio-char adsorbents for different

Table 3
Kinetic parameters of different multiple heavy metal ions onto microalgae bio-chars obtained from the pseudo-first-order and pseudo-second-order models.

System		Pseudo-first-order			Pseudo-second-order		
		q_e (mg g^{-1})	k_1 (min^{-1})	R^2	q_e (mg g^{-1})	k_2 (g mg^{-1}·min^{-1})	R^2
Cu	MB-OB	131.61	0.061 ± 0.003	0.97	12.50	0.0064 ± 0.0033	0.99
	MB-DOB	148.10	0.0862 ± 0.005	0.96	14.86	0.0010 ± 0.0025	0.99
Ni	MB-OB	105.63	0.058 ± 0.004	0.95	10.63	0.0012 ± 0.0016	0.99
	MB-DOB	133.43	0.096 ± 0.005	0.97	11.11	0.0016 ± 0.0018	0.99
Co	MB-OB	117.91	0.071 ± 0.0004	0.97	10.86	0.0019 ± 0.0022	0.99
	MB-DOB	101.32	0.090 ± 0.011	0.88	10.63	0.0016 ± 0.0021	0.99
Cd	MB-OB	132.95	0.070 ± 0.005	0.94	10.32	0.0014 ± 0.0028	0.99
	MB-DOB	136.48	0.086 ± 0.009	0.91	12.11	0.0010 ± 0.0032	0.99

Table 4
Langmuir and Freundlich model to adsorption isotherms.

System		Langmuir			Freundlich		
		q_e (mg g^{-1})	K_L (L·mg^{-1})	R^2	K_F (mg·g^{-1})	n	R^2
Cu	MB-OB	12.5	0.57 ± 0.12	0.99	6.68 ± 0.08	9.43 ± 0.01	0.86
	MB-DOB	14.08	0.157 ± 0.36	0.99	4.80 ± 0.09	12.19	0.92
Ni	MB-OB	10.30	0.30 ± 0.34	0.99	6.04 ± 0.07	9.91 ± 0.01	0.88
	MB-DOB	11.90	0.31 ± 0.20	0.99	7.76 ± 0.04	33.74	0.90
Co	MB-OB	9.09	0.50 ± 0.38	0.99	5.78 ± 0.054	9.25 ± 0.05	0.94
	MB-DOB	9.43	0.75 ± 0.69	0.99	4.66 ± 0.01	17.24	0.88
Cd	MB-OB	8.33	0.39 ± 0.22	0.99	5.26 ± 0.04	9.09 ± 0.01	0.96
	MB-DOB	11.11	0.21 ± 0.32	0.99	2.65 ± 0.12	9.09 ± 0.01	0.90

times (10, 30, 60, 90, 120, 180, 240, 480, 720, and 1440 min) and the results are depicted in Fig. 9. It can be observed that the adsorption rate was initially fast and could achieve greater than 70% and 80% of maximum adsorption capacity within 240 min for MB-OB and MB-DOB adsorbents, respectively, and attained equilibrium in 480 min with more than 96% with both adsorbents. Also, data shows better adsorption with the MB-DOB compared to MB-OB due to the presence of more pores which are generated by the removal of oil from the algae. During the study, a fast adsorption rate was observed in the initial stage compare to a later stage and this might be due to a significant number of readily available adsorption sites for heavy metals on the adsorbent surface. Thus, for further adsorption experiments, 480 min was preferred as the optimum contact time. Kinetic analysis was performed to understand the different adsorption behaviors in multiple heavy metal systems and to find out a suitable kinetic model. This model elucidates the acquired results and gives information about the adsorption mechanism of heavy metals onto MB-OB and MB-DOB.

3.12. Adsorption kinetics

Two different types of kinetic models which are pseudo-first-order (PFO) and pseudo-second-order (PSO) models mostly used to explain the behavior of adsorption. These models believe that the adsorption rate of metals adsorbed on sorbents surface is proportional to the number of unoccupied sites. The PFO kinetics model is controlled by the physical process, and the PSO kinetics model is controlled by chemical processes, including valence forces sharing or exchanging electrons between the adsorbent and adsorbate. The mathematical models of PFO and PSO are described in Eqs. 8 and 9 (Verma et al., 2020).

$$\ln(q_e - q_t) = \ln q_e - k_1 t \tag{8}$$

$$\frac{t}{q_t} = \frac{1}{k_2 q_e^2} + \frac{t}{q_e} \tag{9}$$

Where q_t and q_e are the amounts of heavy metal ions adsorbed at time t and at equilibrium, respectively (mg/g). k_1 (min^{-1}) and k_2 (g mg^{-1}·min^{-1}) are the adsorption rate constants of PFS and PSO, respectively. The plots of PFO and PSO for all heavy metals are shown in Figs. S6 and 10, respectively, and the estimated kinetic constants are shown in Table 3. Data shows that the correlation coefficient (R^2) of PSO is well fitted in comparison to the PFO kinetic correlation coefficient, which assumes that the adsorption of multiple heavy metals on MB-OB and MB-DOB adsorbents surfaces is a chemical adsorption method, such as valence forces sharing or exchanging electrons between the adsorbent and adsorbate. The calculations for the Langmuir and Freundlich isotherm model of the adsorption behaviors in multiple heavy metal systems for bio-chars are given in Table 4.

3.13. Effect of initial concentrations and isotherms

The study of the initial concentrations provides a substantial clarification of the competition between the four different heavy metals during the adsorption process. The adsorption capacity of both adsorbents for all different four metals is shown in Fig. 11. From the data, it is clear that the adsorption capability of all heavy metals was greater for MB-DOB in comparison to the MB-OB. The adsorbents have the same priority for heavy metals, such as Cu(II), Ni(II), and Cd(II) metal ions, and the adsorption of Co(II) was some lower than that of the other metals, possibly because of the competition between the heavy metals.

Two different isotherm models i.e. Langmuir and Freundlich were used to find out the information for the reaction mode between the adsorbent surface and adsorbate ion. The linearized Langmuir equation is defined according to Eq. (10):

$$\frac{C_e}{q_e} = \frac{1}{K_L q_m} + \frac{C_e}{q_m} \tag{10}$$

Freundlich isotherm in the linearized form is expressed in Eq. (8) that can be written in linearized form according to Eq. (11):

$$\ln q_e = \ln K_F + \frac{1}{n} \ln C_e \tag{11}$$

Where q_m and q_e are the maximum adsorption capacity of metals on adsorbent (mg/g), k_L is the Langmuir adsorption constant (L/mg), and K_F and n are Freundlich constants, demonstrating the adsorption ability and adsorption intensity, respectively. The results indicate that the data conforms to the Langmuir adsorption isotherm model (Fig. 12). The Freundlich results are shown in the supplementary information (Fig. S7).

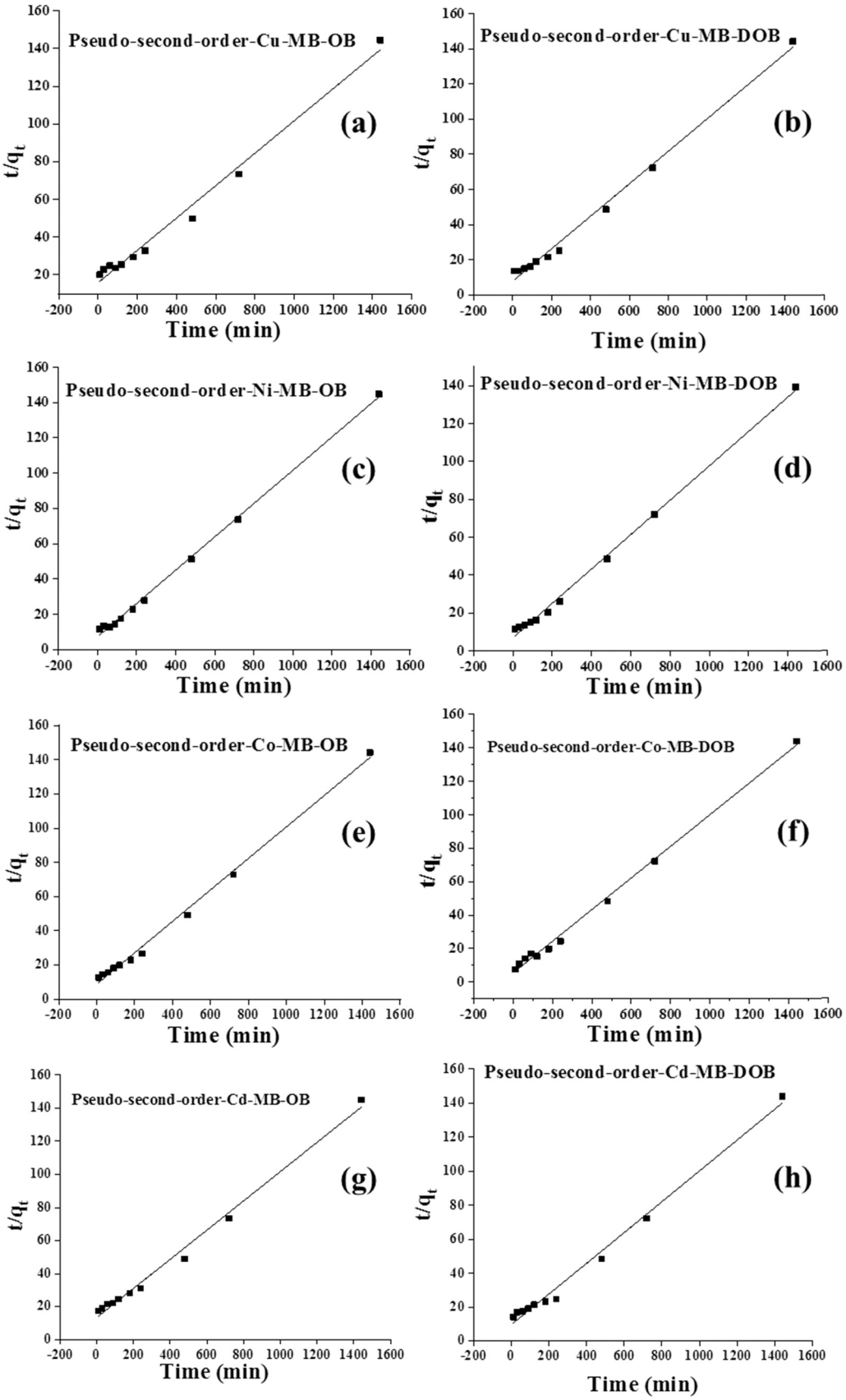

Fig. 11. Pseudo-second-order kinetic models of adsorption behavior for microalgae bio-chars.

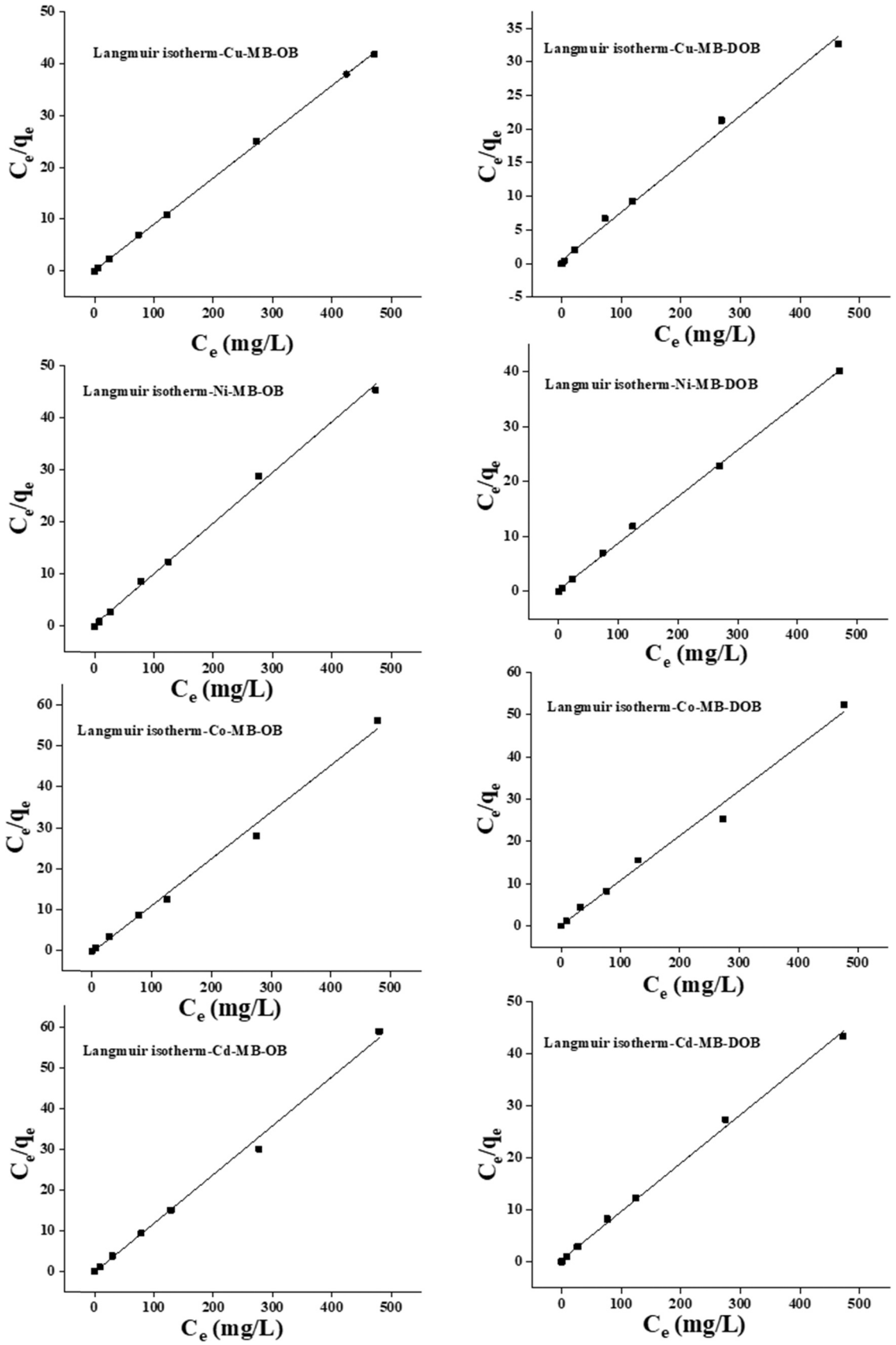

Fig. 12. Langmuir isotherm for microalgae bio-chars.

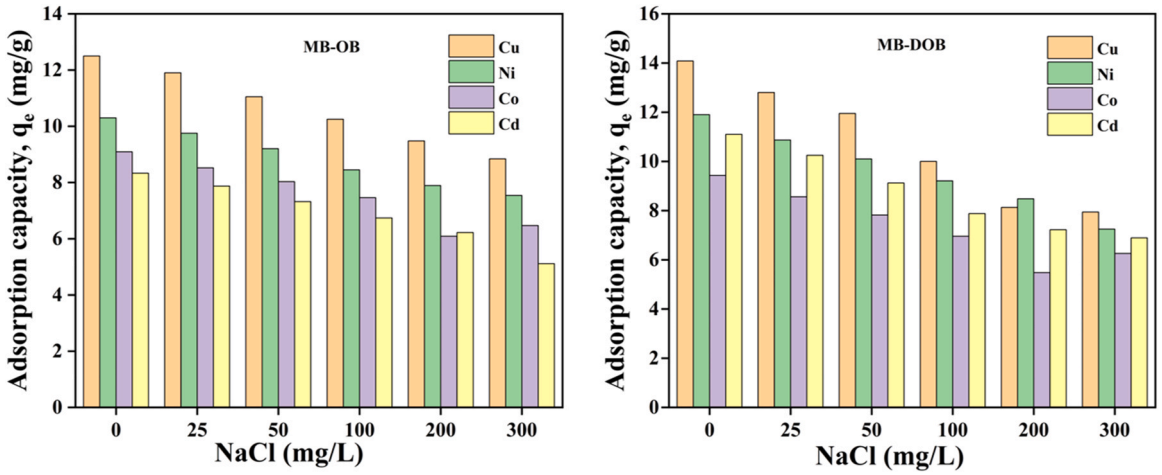

Fig. 13. Effect of NaCl ions on the adsorption.

The different relative parameters along with the correlation coefficient (R^2) are listed in Table 4. The result shows that the experimental data are in agreement with the Langmuir adsorption model, signifying that the adsorption of heavy metal ions in a monolayer adsorption manner.

3.14. Effect of ionic strength

Adsorption of heavy metal ions is also affected by ionic strength. Fig. 13 and S8 show the effect of NaCl (as co-ions) on the adsorption capacity of Cu(II), Ni(II), Co(II), and Cd(II) metal ions on MB-OB and MB-DOB adsorbents. The adsorption capacity decreases as the concentration of NaCl ions increases. Therefore, a considerable effect on the interaction between adsorbate and adsorbent occurs with increasing the concentration of coexisting ions concentration in the solid/liquid interface. The reason behind decreasing adsorption capacity in presence of the co-ions is the screening effect of electrostatic interactions between the adsorbent and adsorbate, or by the competition between the coexisting cations and heavy metal ions for charged adsorption sites. Also, increasing the concentration of co-existing ions decreases the interface potential and thickness of the electric double layer, decreasing the electrostatic adsorption between the adsorbent and the adsorbate (Islam et al., 2011; Xiao et al., 2017).

3.15. Multiple heavy metals remediation efficiencies of bio-chars in the real water sample (municipal wastewater)

In order to verify the feasibility of the practical application of microalgae bio-chars for the removal of multiple heavy metals from the real water sample, adsorption tests were performed using municipal wastewater. Prior to the start of adsorption tests, the freshly collected municipal wastewater was analyzed for the presence of heavy metal contaminants in the untreated municipal wastewater sample. The quantitative analysis of selected heavy metals revealed the presence of Ni (18.50 ± 0.27 ppb), Cu (34.06 ± 0.58 ppb), Pb (22.70 ± 0.92 ppb), and Zn (56.55 ± 0.17 ppb). The bio-char (MB-OB and MB-DOB) remediation efficiencies of multiple heavy metals were tested against the aforementioned heavy metals.

Fig. 14 shows the multiple heavy metal removal efficiency of bio-char MB-OB and MB-DOB. Statistics (mean ± SD) for the remediation efficiency of multiple heavy metals at 60, 120, 240, 480, and 720 min are given in Table S10. The result demonstrates the efficient removal of heavy metals (Cu, Ni, Pb, and Zn) ~ 97–98% in 240 min and ~ 99–100% in 480 min using MB-DOB. Taking into account, the efficiency of removing heavy metals (Cu, Ni, Pb and Zn) using MB-OB was observed as ~ 80% 99% in 240 min and ~ 98% 100% in 480 min. The complete removal (unobserved concentration) of heavy metals has been observed in 720 min in both the bio-chars Mb-OB and MB-DOB. The result indicates a similar pattern of heavy metals removal from municipal wastewater as seen in the prepared multiple heavy metal solution systems. Furthermore, in contrast to the removal efficiency in the multiple

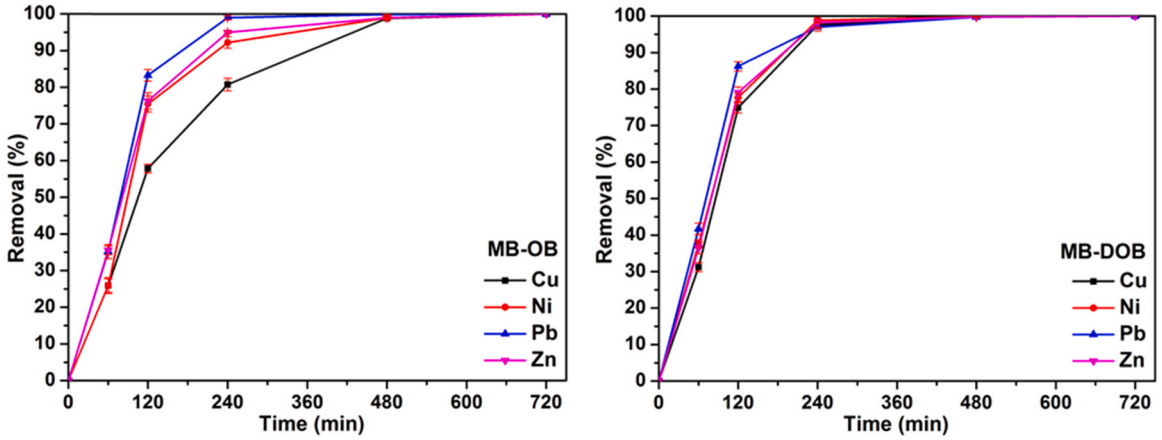

Fig. 14. Multiple heavy metals remediation efficiencies of bio-chars in MWW.

heavy metal solution, the removal efficiency indicates a shorter duration of time for efficient heavy metal removal in municipal wastewater. This could be due to the lower concentration of heavy metals in the real wastewater sample (municipal wastewater) compared to the prepared multiple heavy metal solution systems. The results of heavy metal adsorption tests in municipal wastewater promote the possibility of a realistic application for wastewater remediation.

4. Conclusion

This study investigated the microalgae cultivation for biomass generation and wastewater remediation synergistically in the municipal wastewater integrated HRAP system. Also, the microalgae biomass was applied to produce eco-friendly bio-chars and bio-oils via the HTCL process. The XRD of bio-chars revealed the evolution of graphitic 2H indexing plane structures with a crystalline phase presence in microalgae bio-chars. Raman spectroscopy revealed the higher I_D/I_G ratio of graphitic phase presence in MB-DOB signifying highly disordered graphitic structure due to the high C/N and low C/H ratio compare to the MB-OB. The FTIR spectra evidenced the pyridinic, pyrrolic, and quaternary structures with graphitic configurations in the bio-chars obtained from the microalgae biomass. The appearance of carbonyl functionalities in bio-chars supported the competence to adsorb heavy metal ions on surfaces. The electron micrograph revealed the creation of micro-rods and flakes like morphology with remarkable high surface area in MB-DOB. Besides, the microalgae bio-oils obtained from the HTCL process exhibited that aliphatic protons are mostly prevailing, whereas protons proximal to heteroatoms (alcohols, carbohydrates) are highly intense in BO-DOB as analyzed in ^{1}H NMR. The multiple heavy metals remediation of MB-DOB revealed better efficiency ~100% in 720 min compare to MB-OB. Moreover, two different types of kinetic models, i.e. pseudo-first-order and pseudo-second-order models were used to explain the adsorption behavior and the adsorption rate of bio-chars in multiple heavy metal systems viz. Cu(II), Ni(II), Co(III), and Cd (II). Langmuir and Freundlich's model fitted well to adsorption isotherms. The results of the study have demonstrated a potential for multiple heavy metals removal alongside microalgae bio-oils as an eco-friendly approach.

Funding

This research work was carried out under the Indo-Russian-INT/RUS/RFBR/347 research grant supported by DST, Government of India.

CRediT authorship contribution statement

Krishna Kumar Jaiswal: Conceptualization, Methodology, Software, Validation, Formal analysis, Investigation, Writing - original draft, Visualization. **Vinod Kumar**: Conceptualization, Writing - review & editing, Supervision. **Ravikant Verma:** Methodology. **Monu Verma:** Writing - review & editing. **Arvind Kumar:** Methodology. **Mikhail S. Vlaskin**: Conceptualization, Writing - review & editing. **Manisha Nanda**: Writing - review & editing. **Hyunook Kim:** Writing - review & editing.

Declaration of Competing Interest

The authors declare that they have no known competing financial interests or personal relationships that could have appeared to influence the work reported in this paper.

Acknowledgment

The authors are grateful to the Central Instrumentation Facility, Pondicherry University for LASER-Raman, FTIR, SEM, BET, CHNS, ^{1}H NMR, and ICS characterizations.

Appendix A. Supporting information

Supplementary data associated with this article can be found in the online version at doi:10.1016/j.jhazmat.2020.124987.

References

Ahmad, M., Ahmad, M., Usman, A.R., Al-Faraj, A.S., Abduljabbar, A., Ok, Y.S., Al-Wabel, M.I., 2017. Date palm waste-derived biochar composites with silica and zeolite: synthesis, characterization and implication for carbon stability and recalcitrant potential. Environ. Geochem. Health 41, 1–18.

APHA, A.W.W.A., 2012. Standard Methods for Examination of Water and Wastewater, 22nd ed..,. American Public Health Association,, Washington.

Arora, N., Jaiswal, K.K., Kumar, V., Vlaskin, M.S., Nanda, M., Pruthi, V., Chauhan, P.K., 2020. Small-scale phyco-mitigation of raw urban wastewater integrated with biodiesel production and its utilization for aquaculture. Bioresour. Technol. 297, 122489.

Arora, N., Laurens, L.M.L., Sweeney, N., Pruthi, V., Poluri, K.M., Pienkos, P.T., 2019. Elucidating the unique physiological responses of halotolerant Scenedesmus sp. cultivated in sea water for biofuel production. Algal Res. 37, 260–268.

Arora, N., Patel, A., Pruthi, P.A., Pruthi, V., 2015. Synergistic dynamics of nitrogen and phosphorous influences lipid productivity in Chlorella minutissima for biodiesel production. Bioresour. Technol. 213, 79–87.

Bligh, E.G., Dyer, W.J., 1959. A rapid method for total lipid extraction and purification. Can. J. Biochem. Physiol. 37, 911–917.

Boateng, A.A., Daugaard, D.E., Goldberg, N.M., Hicks, K.B., 2007. Bench-scale fluidized-bed pyrolysis of switchgrass for bio-oil production. Ind. Eng. Chem. Res. 46, 1891–1897.

Bradford, M.M., 1976. A rapid and sensitive method for the quantitation of microgram quantities of protein utilizing the principle of protein-dye binding. Anal. Biochem. 72, 248–254.

Cai, W., Zhao, Z., Li, D., Lei, Z., Zhang, Z., Lee, D.-J., 2019. Algae granulation for nutrients uptake and algae harvesting during wastewater treatment. Chemosphere 214, 55–59.

Cairns, S., Robertson, I., Sigmund, G., Street-Perrott, A., 2020. The removal of lead, copper, zinc and cadmium from aqueous solution by biochar and amended biochars. Environ. Sci. Pollut. Res. 27, 21702–21715.

Cao, X., Harris, W., 2010. Properties of dairy-manure-derived biochar pertinent to its potential use in remediation. Bioresour. Technol. 101, 5222–5228.

Carolin, C.F., Kumar, P.S., Saravanan, A., Joshiba, G.J., Naushad, M., 2017. Efficient techniques for the removal of toxic heavy metals from aquatic environment: a review. J. Environ. Chem. Eng. 5, 2782–2799.

Choudhary, P., Assemany, P.P., Naaz, F., Bhattacharya, A., Castro, J.S., Couto, E.A.C., Calijuri, M.L., Pant, K.K., Malik, A., 2020. A review of biochemical and thermochemical energy conversion routes of wastewater grown algal biomass. Sci. Total Environ. 726, 137961.

Chowdhury, S., Mazumder, M.A.J., Al-Attas, O., Husain, T., 2016. Heavy metals in drinking water: occurrences, implications, and future needs in developing countries. Sci. Total Environ. 569–570, 476–488.

Debono, O., Villot, A., 2015. Nitrogen products and reaction pathway of nitrogen compounds during the pyrolysis of various organic wastes. J. Anal. Appl. Pyrol. 114, 222–234.

Deng, R., Huang, D., Wan, J., Xue, W., Wen, X., Liu, X., Chen, S., Lei, L., Zhang, Q., 2020. Recent advances of biochar materials for typical potentially toxic elements management in aquatic environments: a review. J. Clean. Prod. 255, 119523.

Ding, Z., Hu, X., Wan, Y., Wang, S., Gao, B., 2016. Removal of lead, copper, cadmium, zinc, and nickel from aqueous solutions by alkali-modified biochar: batch and column tests. J. Ind. Eng. Chem. 33, 239–245.

Fan, L., Zhang, H., Li, J., Wang, Y., Leng, L., Li, J., Yao, Y., Lu, Q., Yuan, W., Zhou, W., 2020. Algal biorefinery to value-added products by using combined processes based on thermochemical conversion: a review. Algal Res. 47, 101819.

Hernández-prieto, M.A., Semeniuk, T.A., Giner-lamia, J., Futschik, M.E., 2016. The transcriptional landscape of the photosynthetic model cyanobacterium synechocystis sp. PCC6803. Sci. Rep. 6, 22168.

Hu, X., Nango, K., Bao, L., Li, T., Hasana, M.D.M., Li, C.-Z., 2019. High yields of solid carbonaceous materials from biomass. Green Chem. 21, 1128–1140.

Huang, Q., Song, S., Chen, Z., Hu, B., Chen, J., Wang, X., 2019. Biochar-based materials and their applications in removal of organic contaminants from wastewater: state-of-the-art review. Biochar 1, 45–73.

Huff, M.D., Lee, J.W., 2016. Biochar-surface oxygenation with hydrogen peroxide. J. Environ. Manag. 165, 17–21.

Islam, M.N., Paul, P.K., Hussain, S.A., Bhattacharjee, D., 2011. Layer-by-layer assembling and characterizations of dye-polyions onto solid substrate by electrostatic adsorption process. Int. J. Modern Phys. B 25, 1905–1914.

Jaiswal, K.K., Banerjee, I., Singh, D., Sajwan, P., Chhetri, V., 2020. Ecological stress stimulus to improve microalgae biofuel generation: a review. Octa J. Biosci. 8, 48–54.

Jaiswal, K.K., Kumar, V., Vlaskin, M.S., Sharma, N., Rautela, I., Nanda, M., Arora, N., Singh, A., Chauhan, P.K., 2020. Microalgae fuel cell for wastewater treatment: recent advances and challenges. J. Water Process Eng. 38, 101549.

Jaiswal, K.K., Manikandan, D., Murugan, R., Ramaswamy, A.P., 2018. Microwave-assisted rapid synthesis of Fe_3O_4/poly(styrene-divinylbenzeneacrylic acid) polymeric magnetic composites and investigation of their structural and magnetic properties. Eur. Polym. J. 98, 177–190.

Jaiswal, K.K., Pandey, H., 2014. Next generation renewable and sustainable micro-fuels from Chlorella pyrenoidosa. Int. J. Recent Sci. Res. 5, 767–769.
Jaiswal, K.K., Prasath, R.A., 2016. Integrated growth potential of Chlorella pyrenoidosa using hostel mess wastewater and its biochemical analysis. Int. J. Environ. Sci. 6, 592–599.
Jaiswal, K.K., Sudhakar, S., Ramaswamy, A.P., 2018. 'Graphene' - world's thinnest material for revolutionizing applications. Everyman's Sci. 53, 219–223.
Johansson, C.L., Paul, N.A., de Nys, R., Roberts, D.A., 2016. Simultaneous biosorption of selenium, arsenic and molybdenum with modified algal-based biochars. J. Environ. Manag. 165, 117–123.
Kadir, W.N.A., Lam, M.K., Uemura, Y., Lim, J.W., Lee, K.T., 2018. Harvesting and pretreatment of microalgae cultivated in wastewater for biodiesel production: a review. Energy Convers. Manag. 171, 1416–1429.
Kehrein, P., van Loosdrecht, M., Osseweijer, P., Garfí, M., Dewulf, J., Posada, J., 2020. A critical review of resource recovery from municipal wastewater treatment plants – market supply potentials, technologies and bottlenecks. Environ. Sci.: Water Res. Technol. 6, 877–910.
Kidgell, J.T., de Nys, R., Hu, Y., Paul, N.A., Roberts, D.A., 2014. Bioremediation of a complex industrial effluent by biosorbents derived from freshwater macroalgae. PLoS One 9, e94706.
Kumar, G., Shobana, S., Chen, W.-H., Bach, Q.-V., Kim, S.-H., Atabani, A.E., Chang, J.-S., 2017. A review of thermochemical conversion of microalgal biomass for biofuels: chemistry and processes. Green Chem. 19, 44–67.
Kumar, V., Arora, N., Pandey, S., Jaiswal, K.K., Nanda, M., 2020. Microwave-assisted pre-treatment of harmful algal blooms for microbial oil-centered bio-refinery approach. Biomass Convers. Biorefinery. https://doi.org/10.1007/s13399-020-00941-5.
Lee, X.J., Ong, H.C., Gan, Y.Y., Chen, W.-H., Mahlia, T.M.I., 2020. State of art review on conventional and advanced pyrolysis of macroalgae and microalgae for biochar, bio-oil and bio-syngas production. Energy Convers. Manag. 210, 112707.
Lichtenthaler, H.K., 1987. Chlorophylls and carotenoids: pigments of photosynthetic biomembranes. Methods Enzymol. 148, 350–382.
Liu, H., Ahmad, M.S., Alhumade, H., Elkamel, A., Sammak, S., Shen, B., 2020. A hybrid kinetic and optimization approach for biomass pyrolysis: the hybrid scheme of the isoconversional methods, DAEM, and a parallel-reaction mechanism. Energy Convers. Manag. 208, 112531.
Liu, W.-J., Jiang, H., Yu, H.-Q., 2015. Development of biochar-based functional materials: toward a sustainable platform carbon material. Chem. Rev. 115, 12251–12285.
Ma, Z., Yang, Y., Ma, Q., Zhou, H., Luo, X., Liu, X., Wang, S., 2017. Evolution of the chemical composition, functional group, pore structure and crystallographic structure of bio-char from palm kernel shell pyrolysis under different temperatures. J. Anal. Appl. Pyrolysis 127, 350–359.
Malavasi, V., Soru, S., Cao, G., 2020. Extremophile microalgae: the potential for biotechnological application. J. Phycol. 56, 559–573.
Maliutina, K., Tahmasebi, A., Yu, J., 2018. Effects of pressure on morphology and structure of bio-char from pressurized entrained-flow pyrolysis of microalgae. Data Brief 18, 422–431.
Masuko, T., Minami, A., Iwasaki, N., Majima, T., 2005. Carbohydrate analysis by a phenol-sulfuric acid method in microplate format. Anal. Biochem. 339, 69–72.
Mathimani, T., Baldinelli, A., Rajendran, K., Prabakar, D., Matheswaran, M., van Leeuwen, R.P., Pugazhendhi, A., 2019. Review on cultivation and thermochemical conversion of microalgae to fuels and chemicals: process evaluation and knowledge gaps. J. Clean. Prod. 208, 1053–1064.
Michalak, I., Basladynska, S., Mokrzycki, J., Rutkowski, P., 2019. Biochar from a freshwater macroalga as a potential biosorbent for wastewater treatment. Water 11, 1–16.
Mulders, K.J.M., Lamers, P.P., Martens, D.E., Wijffels, R.H., 2014. Phototrophic pigment production with microalgae: biological constraints and opportunities. J. Phycol. 50, 229–242.
Mullen, C.A., Boateng, A.A., 2008. Chemical composition of bio-oils produced by fast pyrolysis of two energy crops. Energy Fuels 22, 2104–2109.
Mullen, C.A., Strahan, G.D., Boateng, A.A., 2009. Characterization of various fast-pyrolysis bio-oils by NMR spectroscopy. Energy Fuels 23, 2707–2718.
Nirmalakhandan, N., Selvaratnam, T., Henkanatte-Gedera, S.M., Tchinda, D., Abeysiriwardana-Arachchige, I.S.A., Delanka-Pedige, H.M.K., Munasinghe-Arachchige, S.P., Zhang, Y., Holguin, F.O., Lammers, P.J., 2019. Algal wastewater treatment: photoautotrophic vs. mixotrophic processes. Algal Res. 41, 101569.
Park, C.M., Han, J., Chu, K.H., Al-Hamadani, Y.A.J., Her, N., Heo, J., Yoon, Y., 2017. Influence of solution pH, ionic strength, and humic acid on cadmium adsorption onto activated biochar: experiment and modeling. J. Ind. Eng. Chem. 48, 186–193.
Park, J.B.K., Craggs, R.J., Shilton, A.N., 2011. Wastewater treatment high rate algal ponds for biofuel production. Bioresour. Technol. 102, 35–42.
Qin, C., Wang, H., Yuan, X., Xiong, T., Zhang, J., Zhang, J., 2020. Understanding structure-performance correlation of biochar materials in environmental remediation and electrochemical devices. Chem. Eng. J. 382, 122977.
Salama, E.-S., Kurade, M.B., Abou-Shanab, R.A.I., El-Dalatony, M.M., Yang, I.-S., Min, B., Jeon, B.-H., 2017. Recent progress in microalgal biomass production coupled with wastewater treatment for biofuel generation. Renew. Sustain. Energy Rev. 79, 1189–1211.
Seehra, M.S., Geddam, U.K., Schwegler-Berry, D., Stefaniak, A.B., 2015. Detection and quantification of 2H and 3R phases in commercial graphene-based materials. Carbon 95, 818–823.
Sudhakar, S., Jaiswal, K.K., Peera, S.G., Ramaswamy, A.P., 2017. Green synthesis of N-graphene by hydrothermal-microwave irradiation for alkaline fuel cell application. Int. J. Recent Sci. Res. 8, 19049–19053.
Sudhakar, S., Jaiswal, K.K., Ramaswamy, A.P., 2018. The role of microwave irradiation temperature on nitrogen doping in metal-free graphene catalysts for an efficient oxygen reduction reaction in an alkaline condition. ChemistrySelect 3, 8962–8972.
Sutherland, D.L., Ralph, P.J., 2019. Microalgal bioremediation of emerging contaminants - opportunities and challenges. Water Res. 164, 114921.
Tyler, D.N., Wooding, N.S., 1958. The determination and the significance of crystallite size in regenerated cellulose fibres. J. Soc. Dyers Colourist 74, 283–291.
Umamaheswari, J., Shanthakumar, S., 2016. Efficacy of microalgae for industrial wastewater treatment: a review on operating conditions, treatment efficiency and biomass productivity. Rev. Environ. Sci. Bio/Technol. 15, 265–284.
Usman, A.R.A., Abduljabbar, A., Vithanage, M., Ok, Y.S., Ahmad, M., Ahmad, M., Elfaki, J., Abdulazeem, S.S., Al-Wabel, M.I., 2015. Biochar production from date palm waste: charring temperature induced changes in composition and surface chemistry. J. Anal. Appl. Pyrolysis 115, 392–400.
Verma, M., Kumar, A., Singh, K.P., Kumar, R., Kumar, V., Srivastava, C.M., Rawat, V., Rao, G., Kumari, S., Sharma, P., Kim, H., 2020. Graphene oxide-manganese ferrite (GO-$MnFe_2O_4$) nanocomposite: One-pot hydrothermal synthesis and its use for adsorptive removal of Pb^{2+} ions from aqueous medium. J. Mol. Liq. 315, 113769.
Vonshak, A., Cheung, S.M., Chen, F., 2000. Mixotrophic growth modifies the response of Spirulina (Arthrospira) platensis (Cyanobacteria) cells to light. J. Phycol. 36, 675–679.
Wan, M., Liu, P., Xia, J., Rosenberg, J.N., Oyler, G.A., Betenbaugh, M.J., Nie, Z., Qiu, G., 2011. The effect of mixotrophy on microalgal growth, lipid content, and expression levels of three pathway genes in Chlorella sorokiniana. Appl. Microbiol. Biotechnol. 91, 835–844.
Wang, L., Ok, Y.S., Tsang, D.C.W., Alessi, D.S., Rinklebe, J., Wang, H., Mašek, O., Hou, R., O'Connor, D., Hou, D., 2020. New trends in biochar pyrolysis and modification strategies: feedstock, pyrolysis conditions, sustainability concerns and implications for soil amendment. Soil Use Manag. 36, 358–386.
Wang, W.-N., Widiyastuti, W., Ogi, T., Lenggoro, I.W., Okuyama, K., 2007. Correlations between crystallite/particle size and photoluminescence properties of submicrometer phosphors. Chem. Mater. 19, 1723–1730.
Waqas, M., Aburiazaiza, A.S., Minadad, R., Rehan, M., Barakat, M.A., Nizami, A.S., 2018. Development of biochar as fuel and catalyst in energy recovery technologies. J. Clean. Prod. 188, 477–488.
Xiang, W., Zhang, X., Chen, J., Zou, W., He, F., Hu, X., Tsang, D.C.W., Ok, Y.S., Gao, B., 2020. Biochar technology in wastewater treatment: a critical review. Chemosphere 252, 126539.
Xiao, Y., Xue, Y., Gao, F., Mosa, A., 2017. Sorption of heavy metal ions onto crayfish shell biochar: effect of pyrolysis temperature, pH and ionic strength. J. Taiwan Inst. Chem. Eng. 80, 114–121.
Yang, X., Jiang, Y., Xue, B., Xia, M., Luo, F., Xu, S., Li, F., 2019. Microstructure and properties of in-situ prepared cellulosic biomass carbon based diatomite composite. Mater. Sci. Technol. 35, 469–476.
Yang, X., Wan, Y., Zheng, Y., He, F., Yu, Z., Huang, J., Wangh, H., Ok, Y.S., Jiang, Y., Gao, B., 2019. Surface functional groups of carbon-based adsorbents and their roles in the removal of heavy metals from aqueous solutions: a critical review. Chem. Eng. J. 366, 608–621.
Yao, B., Xiao, T., Jie, X., Gonzalez-Cortes, S., Edwards, P.P., 2018. H_2 rich gas production from different leaves. Catal. Today 317, 43–49.
Yuan, J.H., Xu, R.K., Zhang, H., 2011. The forms of alkalis in the biochar produced from crop residues at different temperatures. Bioresour. Technol. 102, 3488–3497.
Yuan, T., Tahmasebi, A., Yu, J., 2015. Comparative study on pyrolysis of lignocellulosic and algal biomass using a thermogravimetric and a fixed-bed reactor. Bioresour. Technol. 175, 333–341.
Zhang, C., Zhang, Z., Zhang, L., Li, Q., Li, C., Chen, G., Zhang, S., Liu, Q., Hu, X., 2020. Evolution of the functionalities and structures of biochar in pyrolysis of poplar in a wide temperature range. Bioresour. Technol. 304, 123002.
Zhang, H., Xu, F., Xue, J., Chen, S., Wang, J., Yang, Y., 2020. Enhanced removal of heavy metal ions from aqueous solution using manganese dioxide-loaded biochar: behavior and mechanism. Sci. Rep. 10, 6067.
Zhao, J.-J., Shen, X.-J., Domene, X., Alcañiz, J.-M., Liao, X., Palet, C., 2019. Comparison of biochars derived from different types of feedstock and their potential for heavy metal removal in multiple-metal solutions. Sci. Rep. 9, 9869.